

How to run on rough terrains

Nihav Dhawale^{1,2}, Shreyas Mandre³, and Madhusudhan Venkadesan^{*1}

¹Department of Mechanical Engineering and Materials Science, Yale University, New Haven, CT 06520

²National Centre for Biological Sciences–Tata Institute of Fundamental Research, Bangalore, Karnataka 560065

³School of Engineering, Brown University, Providence, RI 02912

Abstract

Stability of running on rough terrain depends on the propagation of perturbations due to the ground. We consider stability within the sagittal plane and model the dynamics of running as a two-dimensional body with an alternating aerial and stance phase. Stance is modeled as a passive, impulsive collision followed by an active, impulsive push-off that compensates for collisional losses. Such a runner has infinitely many strategies to maintain periodic gaits on flat ground. However, these strategies differ in how perturbations due to terrain unevenness are propagated. Instabilities manifest as tumbling (orientational instability) or failing to maintain a steady speed (translational instability). We find that open-loop strategies that avoid sensory feedback are sufficient to maintain stability on step-like terrains with piecewise flat surfaces that randomly vary in height. However, these open-loop runners lose orientational stability on rough terrains whose slope and height vary randomly. Only by avoiding tangential collisions is orientational stability recovered. Tangential collisions may be avoided through leg-retraction to match foot and ground speed at touch down. By analyzing the propagation of perturbations, we derive a single dimensionless parameter that governs stability and guides the design and control of both biological and robotic runners.

*Address correspondence to mv@classicalmechanic.net

1 Introduction

Legged terrestrial animals run stably on rough terrains, despite potential difficulties such as sensory latencies and the highly dynamic nature of running. Our current understanding of how running animals negotiate rough terrains is based on studies where the animal experiences obstacles in the form of a single step up or down (Daley et al., 2006; Birn-Jeffery and Daley, 2012), or a random sequence of up and down steps (Grimmer et al., 2008; Voloshina and Ferris, 2015). However, natural terrains exhibit not only variations in height but also in slope, and it is unclear how our understanding of running on step-like terrains translates to such natural terrains.

Mathematical studies of running over rough terrains reflect the experiments and focus on stability when running on step-like terrains that are piecewise flat (Daley and Usherwood, 2010; Blum et al., 2014; Karssen et al., 2015). Furthermore, models of runners with massless legs, such as the spring-legged-inverted-pendulum (SLIP) (Blickhan, 1989; McMahon and Cheng, 1990; Blickhan and Full, 1993), cannot distinguish between different slopes of the terrain and only respond to variations in height. Assuming a massless leg enforces the ground reaction force vector to always align with the leg (Srinivasan and Holmes, 2008) regardless of the terrain’s slope beneath the foot. More detailed models that mimic the anatomy of specific animals or robots avoid this limitation of SLIP models (Karssen et al., 2015), at the cost of generalizability. Thus there is a need for generalizable models of running that incorporate dependence on both terrain slope and height, and yet remain sufficiently abstract to glean principles that may underlie stability on rough terrains.

Stability may be governed by many factors, including sensory feedback control (Pearson, 1993, 1995; Dickinson et al., 2000), the inherently stabilizing mechanical response of the animal’s body (Holmes et al., 2006), energy dissipation within the body (Daley et al., 2006), and feed-forward strategies such as swing-leg retraction (Seyfarth et al., 2003). The slowest is often sensory feedback control that has latencies comparable to or greater than the stance duration. For example, at endurance running speeds for humans, the stance lasts around 200 ms (Cavagna et al., 1964) and only slightly longer than the shortest proprioceptive feedback delay of 70–100 ms or visual feedback delay of 150–200 ms (van Beers et al., 2002). To better understand the inherent stability or instability of the dynamics of running, we consider only passive mechanical and anticipatory strategies in this study without relying on active feedback control.

Studies of running birds and the role of open-loop stability of running find that increased energy dissipation during stance may help stability when faced with an unexpected drop in terrain height (Daley et al., 2006). Consistent with the role of energy dissipation, experiments with humans find that metabolic power increases by 5% to run on step-like terrains versus flat ground (Voloshina and Ferris, 2015). Walking over rough terrains leads to an increase of 28% in metabolic power (Voloshina et al., 2013), higher in both relative and absolute terms. The difference in energetics may indicate that the dynamics of running are inherently less unstable, but such an analysis on natural rough terrains has not been carried out. Therefore, we incorporate energy dissipation in our examination of open-loop strategies to address the effect of dissipation on stability.

Not relying on feedback control within a single stance does not preclude active strategies that rely on anticipation or internal models, sometimes called feed-forward strategies. Computational studies of walking have demonstrated the role of look-ahead strategies that use the height and slope of the oncoming terrain in planning the control (Byl and Tedrake, 2009). Evidence for the importance of feed-forward strategies for running come from computational studies of SLIP-like running dynamics (Seyfarth et al., 2003) that show how swing-leg retraction automatically modulates the landing angle in response to unexpected variations in the terrain height. However, these studies on running have not yet considered the effect of slope variations in the terrain. Thus in our study, we analyze anticipatory strategies that incorporate the slope of the oncoming terrain.

An extreme and simplified approximation of running is that of a point mass with an impulsive and instantaneous stance followed by projectile flight. Such an approximation appears as a natural solution to the problem of minimizing measures of metabolic energy consumption when the desired forward speed exceeds critical levels, and subject to other constraints such as step length (Srinivasan and Ruina, 2006). SLIP-like models are an unfolding of these point-mass instantaneous-stance models to have finite stance duration. They have helped us understand the kinetics of stance (Holmes et al., 2006) and the energetics of producing forces (Srinivasan and Ruina, 2006) on flat terrains, and the role of swing-leg retraction on piecewise flat terrains (Blum et al., 2014). However, these point-mass models possess no sense of body orientation during the aerial phase and are therefore immune to falling by tumbling.

In this study, we unfold the point-mass, instantaneous-stance model by using a finite moment of inertia for the runner, while still maintaining an impulsive stance. A finite moment of inertia defines a body orientation and thus enables the examination of the effect of angular momentum fluctuations induced by stance. Such a model maps the net effect of the ground forces over stance as a linear impulse applied at the contact point and an angular impulse applied at the center of mass. These impulses lead to a change in the linear and angular momentum of the whole runner because of the passive and active forces during stance. As we discuss later, the angular impulse captures the effect of a finite stance duration and configuration changes during stance.

Section 2 develops a sagittal-plane model that incorporates a finite moment of inertia, inelastic 2D collisions, and an active push-off so that both terrain slope and height variations affect stability. In section 3, we use Monte Carlo simulations with random variation of ground height and slope to examine open-loop strategies, the effects of energy dissipation, and strategies that anticipate the slope of the terrain. Section 4 derives the linearized dynamical equations and analyzes their stability. Using the linearization, we find a single dimensionless parameter that governs stability in section 5, which in turn guides morphological design for stability. We conclude in section 6 with a discussion of the limitations and generality of our analyses, its relationship to experimental results, and generate testable predictions for future experiments.

2 Mathematical model of sagittal plane running

We model the runner in the sagittal plane as a rigid body (Fig. 1a) of mass m , radius of gyration r_g , i.e. moment of inertia $I_G = mr_g^2$ about its center of mass, and radius r_ℓ (leg length). All quantities are in units such that $m = 1, r_\ell = 1$ and the acceleration due to gravity $g = 1$. See section 7.5 for notation used in this paper.

2.1 Aerial and stance phases

A single step is comprised of an aerial and a stance phase. The aerial phase is modeled as a drag-free projectile in uniform gravity. Stance involves two successive parts: a passive collision with the ground followed by an active push-off. The passive collision is two-dimensional and parameterized by two coefficients of restitution ϵ_n along the normal to the ground and ϵ_t along the tangent to the ground. The active push-off applies a linear impulse \mathbf{J}_{imp} at the contact point P and a rotational

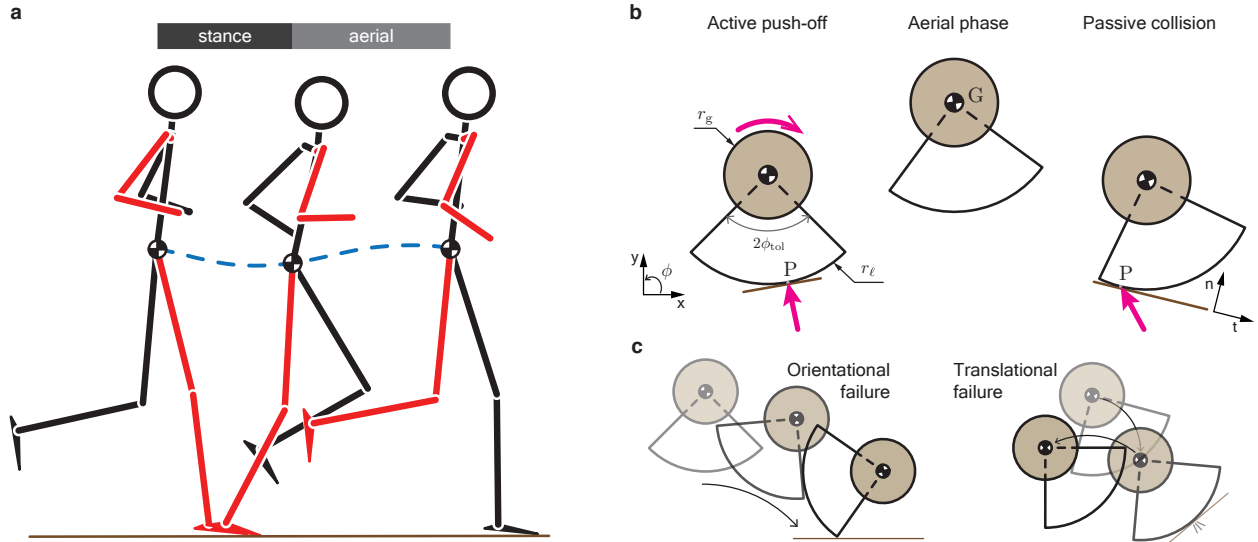


Figure 1: Bouncing as a model of running. **a**, The outline of a human running at 3.5 m/s, created from motion capture data, shows stance and aerial phases over a single step. The stance leg and ipsilateral arm are in red, and the center of mass trajectory is shown as a blue, dashed curve. **b**, The runner pushes-off the ground by applying a linear impulse \mathbf{J}_{imp} at the contact point P, and the effect of additional torques about the center of mass arising from configuration changes during stance are captured by an angular impulse \mathbf{J}_{ϕ} at the center of mass. At the end of the aerial phase, the runner undergoes a passive collision with the ground at the new contact point P. The momentum lost due to the collision in directions tangential and normal to the terrain surface is dictated by the parameters ϵ_t and ϵ_n , respectively. **c**, The runner can fail in two ways: *orientational failure* when orientation at touchdown exceeds the tip-over threshold, i.e. $|\phi^-| > \phi_{\text{tol}}$, or *translational failure* when the forward velocity at take-off drops below a chosen threshold, e.g. $v_{G,x}^+ < 0.01$.

impulse J_ϕ at the center of mass G. The governing dynamical equations are,

$$\text{passive collision: } \mathbf{v}_P^c = \begin{pmatrix} \epsilon_t & 0 \\ 0 & -\epsilon_n \end{pmatrix} \mathbf{v}_P^-, \quad (1a)$$

$$H_{/P}^c - H_P^- = 0, \quad (1b)$$

$$\text{push-off: } \mathbf{v}_G^+ = \mathbf{v}_G^c + \mathbf{J}_{\text{imp}}, \quad I_{/G}\omega^+ = I_{/G}\omega^c + J_{\text{imp},t} + J_\phi, \quad (1c)$$

$$\text{flight: } \ddot{x}_G(t) = 0, \quad \ddot{y}_G(t) = -1, \quad \ddot{\phi}(t) = 0, \quad \text{and} \quad (1d)$$

$$\text{initial conditions: } \begin{pmatrix} x_G(0) \\ y_G(0) \\ \phi(0) \end{pmatrix} = \begin{pmatrix} x_G^+ \\ y_G^+ \\ \phi^+ \end{pmatrix}, \quad \begin{pmatrix} \dot{x}_G(0) \\ \dot{y}_G(0) \\ \dot{\phi}(0) \end{pmatrix} = \begin{pmatrix} v_{G,x}^+ \\ v_{G,y}^+ \\ \omega^+ \end{pmatrix}. \quad (1e)$$

Horizontal and vertical positions are denoted by x and y , respectively, orientation by ϕ , velocity by \mathbf{v} , angular velocity by ω , moment of inertia by $I_{/G}$, and angular momentum by H . Superscript ‘-’ denotes variables immediately preceding the collision, ‘c’ after the passive collision and ‘+’ after the active push-off. Subscripts P and G refer to quantities associated with the foot and center of mass, respectively.

The mechanical state of the runner is parameterized by the center of mass positions (x_G, y_G) , body orientation ϕ , and their respective velocities $(v_{G,x}, v_{G,y})$ and ω . Because the stance is assumed to be instantaneous, the velocities may change discontinuously but the position and orientation remain constant during stance. The instantaneous stance assumption also implies that unmodeled finite forces such as gravity or air-drag do not contribute to the impulse on the runner. However, the active rotational impulse J_ϕ applied at the center of mass G captures the effects of varying posture over stance and the changing center of pressure on the ground. We examine this approximation and its implications in the discussion.

2.2 Stance: passive collision

The runner may control the passive collisional impulse with the ground by varying the parameters ϵ_n and ϵ_t . Because the collisional impulse passes through P, the angular momentum of the runner about the contact point $H_{/P}$ does not change (equation (1b)) and governs the change in the angular velocity ω due to the collision.

The passive normal collision can vary from perfectly inelastic to perfectly elastic, and is parameterized by the normal coefficient of restitution $0 \leq \epsilon_n \leq 1$. The fraction ϵ_n^2 models elastic energy stored and recovered during stance. When $\epsilon_n = 0$, the runner is completely dissipative and $\epsilon_n = 1$ implies perfectly energy conserving.

The tangential coefficient of restitution ϵ_t , parameterizes the tangential impulse when the foot undergoes a collision with the ground. Modulation of ϵ_t is the feature that distinguishes open-loop versus anticipatory strategies in our model. Consider the example where the runner modulates ϵ_t by varying the tangential foot speed at touch-down. The open-loop runner would vary the foot speed by assuming that the terrain is flat and that its own mechanical state matches that of a perfectly periodic and steady speed runner. On a rough terrain the mechanical state and the terrain slope vary from step-to-step. Thus the intended tangential collision ϵ_{tc} and the actual tangential collision ϵ_t may not be equal for the open-loop runner. The anticipatory runner would use information of the terrain’s slope in the oncoming step and its own mechanical state to make sure that the intended and actual foot speed at touchdown match. Thus the actual and the intended (controlled) tangential

collision ϵ_{tc} are equal for the anticipatory runner. The relationship between ϵ_{tc} and ϵ_t are therefore,

$$\epsilon_t = \begin{cases} \epsilon_{tc} \left(\frac{v_{x0}}{v_{P,t}^-} \right) & : \text{open-loop,} \\ \epsilon_{tc} & : \text{anticipatory,} \end{cases} \quad (2)$$

where $v_{P,t}^-$ is the tangential velocity of P just before landing and v_{x0} is the steady forward velocity of the center of mass on flat ground. The two policies are identical on flat ground and when the body has no angular velocity prior to landing. A numerical examination of the relationship between ϵ_{tc} and ϵ_t on rough terrain, is presented in supplement S3.1.

2.3 Stance: active push-off

Stance ends with the application of an active, linear push-off impulse \mathbf{J}_{imp} at the contact point P and an active angular push-off impulse J_ϕ at the center of mass G. We constrain these impulses so that in the absence of external perturbations or other disturbances the runner is perfectly periodic and remains upright ($\phi(t) = 0$) on flat ground. Importantly, once the impulses are chosen for flat ground, they are not allowed to vary step-to-step on any other terrain to reflect the absence of active feedback control. Together, these conditions imply that that the active push-off impulses \mathbf{J}_{imp} and J_ϕ depend only on ϵ_n , ϵ_t , v_{x0} and v_{y0} , and no other parameters, according to

$$\dot{\mathbf{j}}_{\text{imp}} = \begin{pmatrix} v_{x0} \\ v_{y0} \end{pmatrix} - \begin{pmatrix} (\epsilon_t + \frac{1-\epsilon_t}{1+I/G})v_{x0} \\ -\epsilon_n v_{y0} \end{pmatrix}, \quad (3a)$$

$$\dot{j}_\phi = 0. \quad (3b)$$

Thus the center of mass of a periodic runner on flat ground has a constant forward speed v_{x0} and vertical speed v_{y0} at every step.

On rough terrains, there are two options for defining the application of the invariant linear impulse on every step. First, the impulse vector \mathbf{J}_{imp} may be held constant in every step with respect to gravity (x-y frame in Fig. 1a), which we call the *lab-fixed* push-off policy. Second, the impulse vector may be held constant in every step with respect to the normal direction to the terrain at the point of contact (t-n frame in Fig. 1b), which we call a *terrain-fixed* push-off policy. The terrain-fixed policy may be considered a better approximation of what animals do, because the normal to the terrain and the leg orientation are often coupled, whereas leg orientation at contact and gravity may vary from step to step. Implicit in preferring the terrain-fixed policy is the assumption that joint torques to apply forces are planned in an ego-centric (body-fixed) frame of reference. For the disc-like model of a runner that we use, the terrain-fixed and body-fixed policies are identical. Detailed expressions for the velocities in the stance phase, as well as expressions for \mathbf{J}_{imp} under both push-off policies are given in supplement S2. We present an complete analysis of the lab-fixed push-off policy in supplement S9 and focus on the terrain-fixed policy in the main paper.

3 Monte Carlo simulations

A sagittal plane runner can only fail by two modes, when the body orientation exceeds a chosen threshold (*orientational failure*), or by failing to move forward any longer (*translational failure*). We choose the orientational threshold ϕ_{tol} as the angle of tilt to passively topple a human who is standing with their feet apart in a pose resembling double-stance in walking.

We perform Monte Carlo simulations on step-like and undulating rough terrains to estimate the statistics of failure for both open-loop and anticipatory runners. Stability is quantified by the mean steps to failure, like previous studies of rough terrain walking (Byl and Tedrake, 2009).

Runner					Terrain	Monte Carlo		
I/G	ϵ_n	ϕ_{tol}	v_{x0}	v_{y0}	h	λ	M	MAX
0.17	0.63	$\pi/6$	0.96	0.26	$\sim \mathcal{U}(-0.03, 0.03)$	0.1	10^5	10^3

Table 1: Parameter values for a human-like runner. Units are chosen such that $m = 1$, $g = 1$, and $r_\ell = 1$. Parameters describing the runner are discussed in section 2. The heights h at grid points defining the terrain are chosen from a uniform distribution over the range $[-0.03, 0.03]$ (section 7.3). The ensemble size used in the Monte Carlo simulations is M , and MAX is the number of steps to which the runner is simulated. All runners failed before reaching MAX. We elaborate on the choice of these values in section 7.1.

The terrain is modeled as a piecewise linear interpolation of an underlying random grid. The grid points are separated by a distance λ and the heights h of the grid points are chosen from a uniform random distribution (table 1, section 7.3). A linear interpolation between the grid points yields a terrain with random variations in both slope and height. Corners at grid point implies an indeterminate slope, and we therefore define an effective slope at the grid points by interpolating the slope before and after the point (details in section 7.4). Parameter values that represent a human-like runner (table 1) are used for all Monte Carlo simulations, unless indicated otherwise.

3.1 Open-loop runners on rough terrains

Open-loop runners always fail through an orientational instability on rough terrains regardless of the energy dissipated per step (Fig. 2a,d). The open-loop runners with human-like inertia and size take 9.6 ± 4.1 steps (mean \pm standard deviation) before tumbling while only 1% of the runners fall within 3 steps (Fig. 2a). Decreasing ϵ_n from 1 to 0 increases the mean steps to failure by just 2 steps (Fig. 2d). Thus, dissipating more energy per step in the normal collision has minimal influence on stability. The tangential collision, parameterized by ϵ_{tc} , has little or no influence because the contour lines of the mean steps to failure are nearly parallel to the ϵ_{tc} axis (Fig. 2d). Therefore, energy dissipation or modulating the tangential collision are both ineffective stabilization strategies for purely open-loop runners.

3.2 Open-loop runners on step-like terrains

The purely open-loop runner remains stable on step-like terrains that are piecewise flat and possess only height variations (Fig. 2b). This is because forward and vertical dynamics are decoupled on piecewise flat terrains, and hence the open-loop runner does not fall as long as the step height is smaller than the apex height of the aerial phase. This result suggests a foot placement strategy for running on any rough terrain, namely to aim to land on flat patches of the ground so that stability is maintained with little reliance on feedback control. However, such a strategy would require visual surveying of the terrain up ahead and planning the location of foot falls. Increased footfall probability on flat regions of the terrain, along with low probability of footfalls on highly sloped regions of the terrain may be evidence for such a foot placement strategy in experiments.

3.3 Effect of terrain geometry

The exact step-to-step variation in the terrain’s height and slope depend on the distribution function used to generate the random terrain (Fig. 2e, inset). However, we find that the distribution underlying the rough terrain has little effect on the distribution of the steps to failure (Fig. 2e) when assessed using three different functions to generate rough terrains: von Mises, uniform and beta. Runners took 9.6 ± 4.1 (mean \pm std. dev.) steps before tumbling on terrains characterized by

von Mises and uniform distributions, and 10.8 ± 4.7 steps on the terrains characterized by the beta distribution. All steps to failure distributions are unimodal, but skewed. A Markov model for the step-to-step dynamics (supplement S7) lends insight into the nearly invariant shape of the steps-to-failure distribution. The insensitivity may arise from the terrain roughness being uncorrelated from step-to-step (terrain’s correlation length $\lambda \ll 1$), and thus the net effect of the perturbations resembles a Gaussian noise process that is propagated by the dynamics of running.

3.4 Anticipatory runners on rough terrains: tangential collisions

Runners that use anticipatory strategies to control the tangential passive collision maintain orientational stability if they entirely avoid tangential collisions using $\epsilon_{tc} = 1$. But these runners eventually fail by completely losing forward momentum (Fig. 2c). Recall that because of the active push-off, the loss of forward momentum is not simply a break of symmetry by the passive tangential collision. Through a more careful analysis, we find that the mean slope encountered by the runners is positive and not zero, i.e. the terrain preferentially impedes the forward momentum (supplement Fig. S10d). For human-like parameters, anticipatory runners take 75 ± 40.9 (mean \pm std. dev) steps before completely losing forward momentum and only 1% of the runners stop moving forward within 15 steps. In contrast, over 80% of the open-loop runners fail within 15 steps.

For the anticipatory runner, permitting tangential collisions $\epsilon_{tc} < 1$ induces orientational failures and the mean steps to failure decreases. For example, with $\epsilon_n = 0$ the mean steps to failure when $\epsilon_{tc} = 1$ is 85 and decreases to 20 when $\epsilon_{tc} = 0.95$ (Fig. 3a). A 5% decrease in ϵ_{tc} caused an over three-fold decrease in the mean steps to failure. Importantly, the dominant mode of failure switches from translational failures to orientational failures (supplement Fig. S5a). At $\epsilon_{tc} = 0$ and independent of ϵ_n , the anticipatory and open-loop strategies are identical. Thus the anticipatory runner substantially improves stability by avoiding tangential collisions.

Increasing energy dissipation in the normal collision increases the number of steps taken by the anticipatory runner. For example, at $\epsilon_{tc} = 1$, where runners only fail by losing forward speed, increasing energy dissipation by changing from $\epsilon_n = 1$ to $\epsilon_n = 0$, increases the mean number of steps taken before failure by two-fold, from 40 to 85 (Fig. 3a). Away from $\epsilon_{tc} = 1$, energy dissipation has a smaller effect on stability. When $\epsilon_{tc} \approx 0$, the anticipatory runners resemble the open-loop runners and the mean steps to failure increases by only 2 steps despite ϵ_n decreasing from 1 to 0 (Fig. 3a). Thus, for the anticipatory runner using $\epsilon_{tc} \approx 1$, increasing energy dissipation in the direction normal to the terrain is an effective means to improve stability, unlike for the open-loop runner.

3.5 Noise in anticipatory strategies

The sensitivity of the steps to failure with respect to tangential collisions prompts an examination of the effect of stochasticity in how a runner may control the tangential collision. After all, no runner can exactly control the tangential collision from step-to-step. For example, errors in sensing the terrain profile as well as motor noise may prevent accurate implementation of a desired ϵ_{tc} . We model such sources of noise in controlling the tangential collision as

$$\epsilon_{t,\text{noisy}} = \epsilon_{tc} + \Delta\epsilon_t\eta, \tag{4a}$$

$$\text{where } \eta \sim \mathcal{U}[-1, 1], \Delta\epsilon_t \in \mathbb{R}. \tag{4b}$$

The uniformly distributed zero-mean random variable η models random step-to-step noise in ϵ_{tc} and $\Delta\epsilon_t$ is the noise intensity.

We find that incurring tangential collisions ($\epsilon_{tc} < 1$) is optimal when there is non-zero noise ($\Delta\epsilon_t > 0$). This is unlike the noiseless anticipatory runner whose optimum is $\epsilon_{tc} = 1$. However, noise in controlling tangential collisions does affect stability and the mean steps to failure are

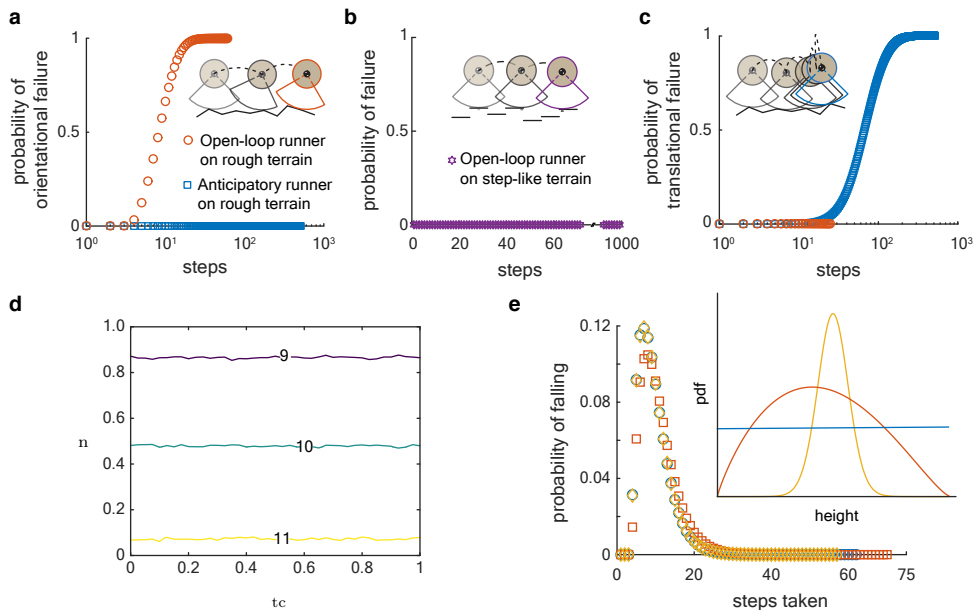


Figure 2: The effect of the tangential collision, energy dissipation and terrain geometry on running stability for a human-like runner, found using Monte Carlo simulations. **a**, Open-loop runners with $\epsilon_{tc} = 0$ (orange circles) lose orientational stability on the rough terrain while anticipatory runners with $\epsilon_{tc} = 1$ (blue squares) maintain orientation. **b**, On the step-like terrain, open-loop runners (purple star) maintain forward speed and orientation as the probability of failure, orientational or translational, is zero. Open-loop and anticipatory runners are identical on step-like terrains **c**, Anticipatory runners slow down on the rough terrain, eventually completely losing forward speed. Whereas human-like open-loop runners also lose forward speed, they lose orientational stability before completely losing forward momentum. **d**, A contour plot of mean steps taken by open-loop runners as a function of ϵ_{tc} and ϵ_n finds that contours are approximately parallel to the ϵ_{tc} axis, while the steps taken increases with decreasing ϵ_n . **e**, Steps to failure distributions for human-like open-loop runners on rough terrain with height distributions for the grid points drawn from von Mises (yellow diamond, mean = 0, $\kappa = 6$), Beta (orange square, $\alpha = 1.9$, $\beta = 2.3$) and uniform distributions (blue circle). The inset shows the probability density functions for the three distributions used to generate the terrain: von Mises (yellow), Beta (orange) and uniform (blue). The distributions were scaled and shifted such that mean height = 0, and range = $0.060r_\ell$ (table 1, section 7.1).

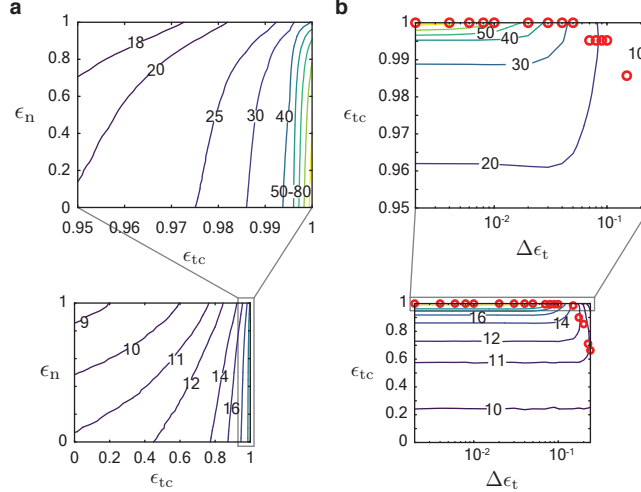


Figure 3: Effect of tangential collisions and energy dissipation on running stability for anticipatory runners. In each panel, the contour plot of mean steps taken over the entire range of independent parameters is shown together with a zoom-in of contours that are bunched together. **a**, The contour plot of mean steps taken by anticipatory runners as a function of ϵ_{tc} and ϵ_n shows that contours are bunched close together around $\epsilon_{tc} \simeq 1$, with the maximum steps taken at $\epsilon_n = 0, \epsilon_{tc} = 1$ (top plot) and minimum at $\epsilon_n = 1, \epsilon_{tc} = 0$ (bottom plot). **b**, Effect of noise in ϵ_{tc} . Contour plot of mean steps taken as a function of ϵ_{tc} and $\Delta\epsilon_t$. The optimal ϵ_{tc} (red circles) is shown for each value of $\Delta\epsilon_t$ simulated.

severely reduced (Fig. 3b). For example, compared to a noiseless human-like runner, the mean steps to failure drops nine-fold for a runner with noise intensity $\Delta\epsilon_t = 0.1$, and the optimum ϵ_{tc} decreases by 1% to $\epsilon_{tc} = 0.99$ (Fig. 3b). Additional noise in the tangential collision of open-loop runners reduces the number of steps taken, but does not alter the dependence of steps taken on ϵ_{tc} (supplement S3.2). Therefore, for anticipatory runners, noise in controlling the tangential collision implies that incurring a slight tangential collision is optimal but at the cost of stability.

3.6 Predictions for ϵ_t in experiments

A main finding of our analyses is the importance of minimizing tangential collisions with the ground when running on rough terrains. But measuring ϵ_t on rough terrains is challenging because it needs a well-defined point of contact under the foot, precise knowledge of the terrain's slope in 3D at that point, and measurement of the reaction force along that tangent. To facilitate comparisons with experimental data, we consider an easier to measure correlate of ϵ_t via the parameter $\hat{\epsilon}_t$ that is defined as

$$\hat{\epsilon}_t = 1 - \frac{\Delta v_x}{v_x}, \quad (5)$$

where $\Delta v_x/v_x$ is the fraction of the forward momentum of the runner lost due to the passive collision. On perfectly flat terrain, $\epsilon_t = \hat{\epsilon}_t$.

In the Monte Carlo simulations, $\hat{\epsilon}_t$ is characterized by a distribution that evolves with increasing steps (Fig. 4a, supplement Fig. S6a). The dependence of $\hat{\epsilon}_t$ on steps taken arises because the runner is slowing down, and thus v_x and consequently Δv_x change from step-to-step. But, the mean of $\hat{\epsilon}_t$ appears to converge to a constant after just 3 steps for all values of ϵ_{tc} (supplement Fig. S6b). Importantly, mean $\hat{\epsilon}_t$ increases linearly with ϵ_{tc} (Fig. 4b) and is this a reliable correlate of the true tangential collision. However, $\hat{\epsilon}_t$ has a reduced range; mean $\hat{\epsilon}_t = 0.81$ at $\epsilon_{tc} = 0$, and mean $\hat{\epsilon}_t = 0.97$

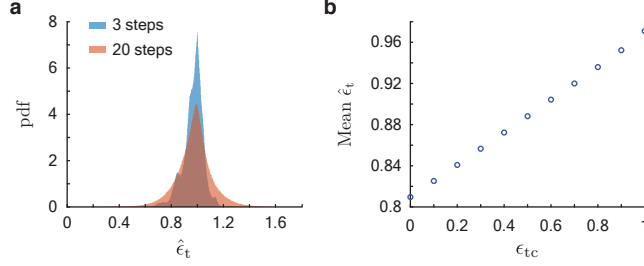


Figure 4: Estimated tangential coefficient of restitution $\hat{\epsilon}_t$ for anticipatory runners using Monte Carlo simulations with an ensemble size of 10^6 . **a**, Probability density function of $\hat{\epsilon}_t$ for human-like anticipatory runners with $\epsilon_{tc} = 1$ on rough terrain after 3 steps and after 20 steps. While the standard deviation almost doubles between the two distributions shown here (supplement Fig. S6c), the mean of the distribution converges by 3 steps (supplement Fig. S6b). **b**, Mean $\hat{\epsilon}_t$, converges by 3 steps for all values of ϵ_{tc} (supplement Fig. S6b), and is always less than 1, ranging from 0.81 at $\epsilon_{tc} = 0$ to 0.97 at $\epsilon_{tc} = 1$.

at $\epsilon_{tc} = 1$. The standard deviation of the distributions converges to a value between 0.05 and 0.1 by approximately 10 steps for most values of ϵ_{tc} except when $\epsilon_{tc} \rightarrow 1$ (Fig. 4a, supplement Fig. S6b). For comparison, reported values of $\hat{\epsilon}_t$ from experiments with human runners on flat and two rough terrains are 0.94 ± 0.01 (mean \pm standard deviation) identically (Dhawale and Venkadesan, 2018). These experimental data are consistent with the prediction that optimal anticipatory runners should maintain $\epsilon_{tc} = 1$.

3.7 Modulation of ϵ_t

The tangential collisional impulse depends on the speed of the foot at collision and also on how that collisional impulse is transmitted to the center of mass. For example, the foot collision may not affect the center of mass very much if the intervening joints between the foot and the body are compliant. The transmission of collisions is treated in terms of sprung and unsprung masses in models of automobiles and in running biomechanics (McGeer, 1990). If collisional impulses at the foot are faithfully transmitted to the center of mass, the retraction rate ω_{ret} is related to ϵ_t as,

$$\epsilon_t = \frac{\omega_{ret}}{v_{p,t}^-}, \quad (6a)$$

$$\text{where } \omega_{ret} = \begin{cases} \epsilon_{tc} v_{p,t}^- & : \text{ anticipatory,} \\ \epsilon_{tc} v_{x0} & : \text{ open-loop} \end{cases}. \quad (6b)$$

Using leg retraction to control ϵ_t implies that the optimal retraction rate zeros the tangential foot speed at landing. Equivalently, the foot may be allowed to collide with the ground and yet achieve $\epsilon_t \approx 1$ by maintaining low stiffness in the leg's joints.

4 Linear stability analysis

For periodic dynamic systems linear stability is defined as the response to small perturbations in the neighborhood of a periodic orbit (Full et al., 2002; Holmes et al., 2006; Bruijn et al., 2013) and analyzed using Floquet theory (Guckenheimer and Holmes, 1983; Holmes et al., 2006). Floquet analysis for the stability of a periodic orbit defines a transverse cross-section to the orbit and a discrete return map from initial conditions on the cross-section back to the same cross-section after a complete period. The eigenvalues of the return map, called Floquet multipliers, are independent of the chosen cross-section and govern the stability of the periodic solution to small perturbations

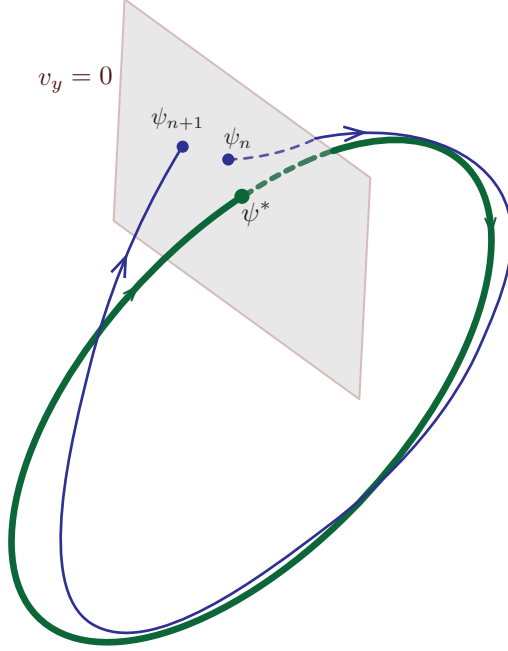


Figure 5: Illustration of the trajectory of the runner in state space in a reference frame that is translating along with the runner with velocity v_{x0} . The runner appears periodic in this reference frame and the runner’s mechanical state follows a periodic orbit. The return map f_{\bullet} (\bullet is ‘ol’ or ‘an’ for open-loop or anticipatory, respectively) is defined from the apex of the aerial phase ($v_y = 0$) to apex of the following aerial phase. ψ^* is the fixed point of the return map and ψ_n is a small perturbation away from the fixed point ψ^* at step n . In the next step, ψ_n maps to ψ_{n+1} at the apex of the following aerial phase under action of the return map f_{\bullet} .

(Guckenheimer and Holmes, 1983). Here we consider the anticipatory runner and discuss the open-loop runner in supplement S5 because the unstable modes of both variants are the same.

The mechanical state of the runner is represented by $\zeta = (x, y, \phi, v_x, v_y, \omega)^T$, where (x, y) and ϕ denote the center of mass position and orientation, and (v_x, v_y) and ω are the respective velocities, all measured in a Newtonian reference frame that translates forward at a constant speed v_{x0} . A steady runner is periodic in this translating Newtonian frame of reference. We define a transverse cross-section (Poincaré section) at the apex of the aerial phase ($v_y = 0$) following the approach of Full et al. (2002) and Seyfarth et al. (2003). The equations (1) yield the step-to-step return map f_{an} and its linearization \mathbf{T}_{an} in terms of a the mechanical state ψ in a translating frame according to

$$\psi = (x, y, \phi, v_x, \omega)^T, \quad (7a)$$

$$\psi_{n+1} = f_{\text{an}}(\psi_n), \quad (7b)$$

$$\Delta\psi_{n+1} = \mathbf{T}_{\text{an}}\Delta\psi_n, \quad (7c)$$

$$\text{where } \Delta\psi = \psi - \psi^*, \quad \mathbf{T}_{\text{an}} = \left. \frac{\partial f_{\text{an}}}{\partial \psi} \right|_{\psi^*}. \quad (7d)$$

The Poincaré map given by equation (7b) has a fixed point at $\psi^* = \mathbf{0}$ when the terrain is flat and corresponds to an exactly periodic runner on flat ground.

The linearized return map \mathbf{T}_{an} has three eigenvalues equal to one and the others are all less

than one. The eigenvalues with magnitude less than one correspond to stable modes so that perturbations along their respective eigenvectors will always decay. The remaining three eigenvalue are all $\lambda = 1$ with algebraic multiplicity equal to 3 and geometric multiplicity equal to 2. This implies that there are only two independent eigenvectors corresponding to the three unity eigenvalues and the matrix \mathbf{T}_{an} is therefore non-diagonalizable. For non-diagonalizable systems, the Jordan decomposition is used to analyze stability in terms of generalized eigenvectors (supplement S5), and implies that the modes (eigenvectors) associated with these eigenvalues cannot be decoupled and analyzed independently.

The two eigenvectors $\boldsymbol{\nu}_1$, $\boldsymbol{\nu}_2$ and the third generalized eigenvector $\boldsymbol{\nu}_3$ corresponding to the repeat eigenvalue $\lambda = 1$ span a subspace in which the dynamics of the return map don't simply decay back to the origin. For a diagonalizable system, any perturbation within this subspace would neither decay nor grow. However, the non-diagonalizable nature of \mathbf{T}_{an} leads to the outcome that a perturbation $\Delta\boldsymbol{\psi}_0$ within this subspace grows with increasing steps. The eigenvectors $\boldsymbol{\nu}_1$, $\boldsymbol{\nu}_2$, $\boldsymbol{\nu}_3$, the initial perturbation $\Delta\boldsymbol{\psi}_0$, and its growth after n steps to $\Delta\boldsymbol{\psi}_n$ are given by,

$$\boldsymbol{\nu}_1 = (0 \ 0 \ 1 \ 0 \ 0)^T, \boldsymbol{\nu}_2 = (1 \ 0 \ 0 \ 0 \ 0)^T, \boldsymbol{\nu}_3 = \left(0 \ 0 \ 0 \ \frac{-1}{\sqrt{2}} \ \frac{1}{\sqrt{2}}\right)^T, \quad (8a)$$

$$\Delta\boldsymbol{\psi}_0 = \sum_{k=1}^3 \alpha_k \boldsymbol{\nu}_k, \text{ and} \quad (8b)$$

$$\Delta\boldsymbol{\psi}_n = n\alpha_3\sqrt{2}\epsilon_n v_{y0}(\boldsymbol{\nu}_1 - \boldsymbol{\nu}_2) + \Delta\boldsymbol{\psi}_0, \text{ respectively.} \quad (8c)$$

As n grows larger, the asymptotic approximation (denoted by \approx) is given by

$$\Delta\boldsymbol{\psi}_n \approx n\alpha_3\sqrt{2}\epsilon_n v_{y0} \begin{pmatrix} -1 \\ 0 \\ 1 \\ 0 \\ 0 \end{pmatrix} \text{ where } n \gg 1. \quad (9)$$

Only a perturbation of magnitude α_3 along $\boldsymbol{\nu}_3$ affects stability and leads to a nearly linear growth within the subspace spanned by the eigenvectors $\boldsymbol{\nu}_1, \boldsymbol{\nu}_2$. Perturbations along $\boldsymbol{\nu}_1$ or $\boldsymbol{\nu}_2$ neither grow nor decay because these represent invariance with respect to rotations and translations of the reference frame, respectively. A perturbation along the generalized eigenvector $\boldsymbol{\nu}_3$ may be geometrically viewed as one that conserves the velocity of the contact point on flat terrain but changes the angular momentum of the runner about its center of mass. Therefore, any perturbation to the angular momentum will affect both orientation and forward speed.

For the special case of the anticipatory runner that completely avoids tangential collisions, the linearized return map \mathbf{T}_{an} with $\epsilon_{tc} = 1$ has eigenvalue $\lambda = 1$ of algebraic multiplicity 4 and geometric multiplicity 2, and one eigenvalue with $|\lambda| < 1$. The eigenvectors $\boldsymbol{\nu}_1, \boldsymbol{\nu}_2$ and the generalized eigenvectors $\boldsymbol{\nu}_3, \boldsymbol{\nu}_4$ associated with $\lambda = 1$ form a basis for a subspace within which an initial perturbation $\boldsymbol{\psi}_0$ grows linearly with the number of steps n in a subspace spanned by eigenvectors

ν_1, ν_2 , i.e.

$$\nu_1 = \begin{pmatrix} 0 \\ 0 \\ 1 \\ 0 \\ 0 \end{pmatrix}, \nu_2 = \begin{pmatrix} 1 \\ 0 \\ 0 \\ 0 \\ 0 \end{pmatrix}, \nu_3 = \begin{pmatrix} 0 \\ 0 \\ 0 \\ 0 \\ 1 \end{pmatrix}, \nu_4 = \begin{pmatrix} 0 \\ 0 \\ 0 \\ 1 \\ 0 \end{pmatrix}, \quad (10a)$$

$$\Delta\psi_0 = \sum_{k=1}^4 \alpha_k \nu_k, \Delta\psi_n = n(\alpha_3 a_1 \nu_1 + \alpha_4 a_2 \nu_2) + \Delta\psi_0, \quad (10b)$$

$$\Delta\psi_n \approx n 2\epsilon_n v_{y0} \begin{pmatrix} \alpha_4 \\ 0 \\ \alpha_3 \\ 0 \\ 0 \end{pmatrix} \text{ for } n \gg 1. \quad (10c)$$

A perturbation to angular velocity ω causes a linear growth in orientation ϕ , and a perturbation to the linear velocity v_x causes a linear growth in position x . However, an anticipatory runner with $\epsilon_{tc} = 1$ avoids angular velocity perturbations due to the terrain altogether, i.e. $\alpha_3 = 0$. Therefore, only forward speed is affected due to the remaining unstable mode ν_4 .

Although there are no unstable eigenvalues with magnitude greater than one, we find that the dynamics of running lead to an unstable growth with increasing steps. The growth due to non-diagonalizability of the return map is linearly proportional to the number of steps, and not geometric as is the case for simple unstable eigenvalues. Importantly, the primary effect of the instability is to affect the forward speed and orientation, consistent with the numerical simulations that use finite perturbations and nonlinear dynamics. Also in agreement with the simulations, the only instability is translational when $\epsilon_{tc} = 1$.

5 Scaling analysis of the orientational failure mode

The mean steps to failure depends on many parameters, but none of the parameters separately predict the failure statistics (supplement Fig. S7). As most runners undergo orientational failures, we investigated whether the amount of body rotation accumulated over a single step due to a terrain slope perturbation would predict failure statistics.

If a runner with a periodic trajectory on flat ground encounters a sloped terrain of angle θ , the orientation ϕ_\bullet at the next landing will no longer be vertical. This orientation ϕ_\bullet accumulated over one step depends on the take-off vertical velocity $v_{y,\bullet}^+$ via the aerial phase time $2v_{y,\bullet}^+$, and take-off angular velocity ω_\bullet^+ , as $\phi_\bullet = 2v_{y,\bullet}^+ \omega_\bullet^+$. The subscript ‘ \bullet ’ is a placeholder for ‘ol’ or ‘an’ as the orientation change depends on whether the runner is purely open-loop (ol) or employs anticipatory (an) control. We hypothesize that the mean steps to failure N_\bullet is a function of the orientational threshold ϕ_{tol} and the orientation change over a single step ϕ_\bullet alone, i.e. $N_\bullet = s_\bullet(\phi_{tol}, \phi_\bullet)$. Substituting the form of $s_\bullet(\phi_{tol}, \phi_\bullet)$ derived in supplement S7, we show that the mean steps to failure N_\bullet is predicted to scale according to,

$$N_\bullet \sim \frac{\phi_{tol}}{\phi_\bullet}, \quad (11)$$

where the expression for ϕ_\bullet is given in supplement equation (S9e).

The mean steps to failure in simulations performed with many different parameter values (supplement S6) are well-approximated by a single function of a dimensionless parameter ϕ_{tol}/ϕ_\bullet .

(Fig. 6). The collapse of the simulation data highlights that the spin accumulated in one step due to a single perturbation (equation (11)) captures the fundamental principle underlying orientational failures. Importantly, this dimensionless parameter collapses the simulation data better than any individual parameter (supplement Fig. S7). Thus, the single parameter $\phi_{\text{tol}}/\phi_{\bullet}$ quantifies stability of runners of different sizes and mass distributions.

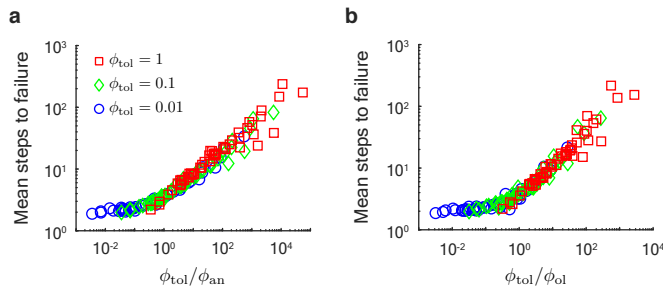


Figure 6: Generalizing results from section 3.1 and section 3.4 to a wider range of physical and terrain parameters. Mean steps to failure from the Monte Carlo simulations is plotted against **a**, $\phi_{\text{tol}}/\phi_{\text{an}}$ and **b**, $\phi_{\text{tol}}/\phi_{\text{ol}}$ for different values of ϕ_{tol} . The mean steps to failure depend mostly on a single dimensionless parameter $\phi_{\text{tol}}/\phi_{\bullet}$. All simulation parameters were varied independently in these simulations. But, for clarity, only variations in ϕ_{tol} are identified with different marker types.

The dimensionless parameter $\phi_{\text{tol}}/\phi_{\bullet}$ also captures the parametric dependence of mean steps to failure on ϵ_{tc} and ϵ_{n} as seen from comparing the contour plots of $\phi_{\text{tol}}/\phi_{\bullet}$ shown in Fig. 7 against that of the direct simulations in Fig. 2d and Fig. 3a. The dependence of mean steps to failure on ϵ_{tc} and ϵ_{n} for small slopes of the terrain is understood using a series expansion of ϕ_{\bullet} in terms of θ as given by,

$$\phi_{\text{ol}} = \left(\frac{2v_{y0}^2}{1 + I/G} \right) \theta + \left(\frac{3 - I/G}{(1 + I/G)^2} + \frac{4I/G}{(1 + I/G)^2} \epsilon_{\text{tc}} + \frac{2}{1 + I/G} \epsilon_{\text{n}} \right) v_{x0} v_{y0} \theta^2 + O(\theta^3), \quad (12a)$$

$$\begin{aligned} \phi_{\text{an}} = & \left(\frac{2v_{y0}^2}{1 + I/G} (1 - \epsilon_{\text{tc}}) \right) \theta + \left(\frac{3 - I/G}{(1 + I/G)^2} + \frac{5I/G - 3}{(1 + I/G)^2} \epsilon_{\text{tc}} - \frac{4I/G}{(1 + I/G)^2} \epsilon_{\text{tc}}^2 + \right. \\ & \left. \frac{2(1 - \epsilon_{\text{tc}})}{1 + I/G} \epsilon_{\text{n}} \right) v_{x0} v_{y0} \theta^2 + O(\theta^3). \end{aligned} \quad (12b)$$

For the open-loop strategy, neither of the collision parameters, ϵ_{n} or ϵ_{tc} , appear in the linear (leading order) term. When using an anticipatory strategy, the tangential collision parameter ϵ_{tc} appears to leading order. The normal collision parameter ϵ_{n} affects the second order dependence on θ for both strategies. These show why it is impossible to avoid orientational failures for the open-loop strategy, but may be avoided when using the anticipatory strategy by choosing $\epsilon_{\text{tc}} = 1$ and $\epsilon_{\text{n}} = 0$.

For the open-loop runner, $\phi_{\text{tol}}/\phi_{\text{ol}}$ is independent of ϵ_{n} and ϵ_{tc} to first order in θ (equation (12a)). Hence the contours in Fig. 7a (which resemble the contours in Fig. 2d from the Monte Carlo simulations) show a weak dependence on ϵ_{n} and ϵ_{tc} that arises from the θ^2 term in equation (12a). The parameter ϕ_{ol} is smallest when $\epsilon_{\text{n}} = \epsilon_{\text{tc}} = 0$, and largest when $\epsilon_{\text{n}} = \epsilon_{\text{tc}} = 1$. For a human-like runner, $I/G \ll 1$ (table 1), and thus the θ^2 term in equation (12a) can be reduced to $(3 + 2\epsilon_{\text{n}})v_{x0}v_{y0}\theta^2$, with no dependence on ϵ_{tc} at the asymptotic limit of $I/G \ll 1$. The asymptotic analysis of ϕ_{ol} therefore explains why the contours of mean steps to failure in the Monte Carlo simulations are nearly parallel to the ϵ_{tc} axis and increase only slightly when ϵ_{n} is decreased (Fig. 2d).

For the anticipatory runner, the first order term in the expansion depends on ϵ_{tc} (equation 12b), unlike the case for the open-loop runner (equation (12a)). Nearly perfect anticipation corresponds

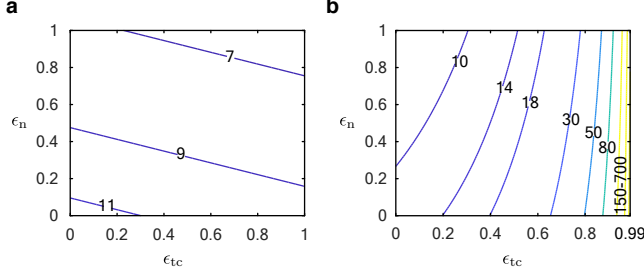


Figure 7: Contour plots of **a**, $\phi_{\text{tol}}/\phi_{\text{ol}}$ and **b**, $\phi_{\text{tol}}/\phi_{\text{an}}$ as a function of ϵ_n and ϵ_{tc} reveal that a single parameter captures the dependence of mean steps to failure of both open-loop runners (Fig. 2d) and anticipatory runners (Fig. 3a) on the collision parameters ϵ_n and ϵ_{tc} . Recall that the only controllable parameters for the runners in these simulations are ϵ_n and ϵ_{tc} . The complete expression for ϕ_{\bullet} , shown in supplement equation (S9e), was used to generate these plots with parameter values drawn from table 1, and $\phi_{\text{tol}} = 1$. For the anticipatory runner, we restricted the maximum value of ϵ_{tc} to 0.99. For higher values of ϵ_{tc} orientational failures are rare and thus not accounted for by $\phi_{\text{tol}}/\phi_{\bullet}$.

to $\epsilon_{\text{tc}} \rightarrow 1$. At this limit $\phi_{\text{an}} \rightarrow 0$ and thus $N = \phi_{\text{tol}}/\phi_{\text{an}} \rightarrow \infty$, explaining why the contours of mean steps to failure in the Monte Carlo simulations are tightly bunched together in the neighborhood of $\epsilon_{\text{tc}} = 1$ (Fig. 3a) and nearly parallel to the ϵ_n axis. Like for the open-loop runner, ϕ_{an} also shows a dependence on ϵ_n only in the θ^2 term of the power series expansion in equation 12b. As ϵ_n decreases so does ϕ_{an} , and thus $\phi_{\text{tol}}/\phi_{\text{an}}$ increases, capturing the trend observed in the Monte Carlo simulations where decreasing ϵ_n increases steps taken for the anticipatory runner (Fig. 3a). For the anticipatory runner, unlike the open-loop runner, the ϵ_n dependence is coupled to ϵ_{tc} , and thus the sensitivity of the parameter $\phi_{\text{tol}}/\phi_{\bullet}$ to changes in ϵ_n depend on the value of ϵ_{tc} . The limit of $\epsilon_{\text{tc}} = 0$, where $\phi_{\text{an}} = \phi_{\text{ol}}$ has already been discussed above, for the open-loop runner. To analyze the case where $\epsilon_{\text{tc}} \rightarrow 1$, we approximate ϕ_{an} in the limit where $I/G \ll 1$ (e.g. human-like runners) as

$$\phi_{\text{an}} \approx 2v_{y0}^2(1 - \epsilon_{\text{tc}})\theta + (1 - \epsilon_{\text{tc}})(2\epsilon_n + 3)v_{x0}v_{y0}\theta^2. \quad (13)$$

To understand the dependence of the mean steps to failure N on ϵ_n and ϵ_{tc} , we consider the limit of small angles of the terrain slope $\theta \ll 1$. Using equation (13), and for small θ we find that mean steps to failure $N = \phi_{\text{tol}}/\phi_{\text{an}}$ and its sensitivity to changes in ϵ_n are given by

$$N = \left(\frac{1}{1 - \epsilon_{\text{tc}}} \right) \frac{\phi_{\text{tol}}}{v_{y0}\theta} (2v_{y0} - 3v_{x0}\theta - 2v_{x0}\theta\epsilon_n), \quad (14a)$$

$$\frac{\partial N}{\partial \epsilon_n} = - \left(\frac{1}{1 - \epsilon_{\text{tc}}} \right) \frac{2\phi_{\text{tol}}v_{x0}}{v_{y0}}. \quad (14b)$$

Therefore, N is more sensitive to changes in ϵ_n when $\epsilon_{\text{tc}} \rightarrow 1$. This resembles Fig. 3a where the mean steps to failure from the Monte Carlo simulations increases significantly as ϵ_n is reduced when $\epsilon_{\text{tc}} \rightarrow 1$, as opposed to when $\epsilon_{\text{tc}} \rightarrow 0$ where there is much lesser sensitivity of the mean steps to failure with respect to changes in ϵ_n .

Improving running stability by increasing mean steps to failure helps provide more time for feedback driven corrections in real-world runners. The analysis of mean-steps to failure in the simplified runners without any feedback ability suggests that increasing ϕ_{tol} and decreasing ϕ_{\bullet} are both effective strategies to negotiate rough terrains. Therefore, besides altering ϵ_{tc} and ϵ_n in order to increase $\phi_{\text{tol}}/\phi_{\bullet}$ as already discussed, increasing I/G and reducing v_{y0} also improves stability.

6 Discussion

We show that purely open-loop strategies with no feedback control cannot stabilize sagittal-plane dynamics during running. Such open-loop runners fail primarily by losing orientational stability and tumbling. Using an anticipatory strategy to eliminate tangential collisions with the ground eliminates orientational instabilities but leads to a steady slowing down of the runner. However, on a step-like piecewise flat terrain the open strategy is sufficient to stabilize the runner without losing forward speed, and so is the anticipatory strategy. If an anticipatory strategy is implemented noisily, i.e. the tangential collisions are low but not entirely eliminated, the runner suffers orientational instabilities. However, both the orientational and the translational instabilities are weak when using an anticipatory strategy and the growth of the instability is only linearly proportional to the number of steps taken and not a higher power. The exact number of steps to failure depend on many parameters including the inertial, geometry, collision parameters and the thresholds in orientation and speed for failure. These large set of parameters may be combined into a single dimensionless parameter that captures the failure statistics, when can also guide the morphological design of stable runners.

Impulsive stance assumption

An impulsive stance phase implies that the stance impulse is defined, but not the detailed time history of forces. Thus the model may be used study the dynamics and stability over multiple steps, but it cannot be used to find the actuation patterns that would achieve the desired impulse. Such simplified models may used to specify the desired collisional and push-off impulses as constraints that should be be met. More detailed models could then be used to calculate the stance force profiles as a constrained search or optimization problem.

The model also ignores the impulse due to the finite forces of gravity, because stance is treated as instantaneous. Relaxing the assumption of instantaneous stance implies that body-weight affects the body’s angular momentum about the contact point according to,

$$H_{/P}^+ - H_{/P}^- = \int_0^{T_{\text{stance}}} M_{/P}(t) dt, \quad (15)$$

where T_{stance} is the stance duration and $M_{/P}(t)$ is the time-varying moment of the body weight about the contact point P. The torque due to gravitational forces about the contact point is proportional to body weight and the time-varying horizontal distance from the center of mass to the contact point. The gravitational contribution is zero for a symmetric stance, and highest for the most asymmetric stance. Assuming a constant forward speed during stance and a 20° touchdown angle, the maximum change in angular momentum about the contact point, i.e. the integral in equation (15), is $|\Delta H_{/P}| \lesssim 0.15$ in the same dimensionless units as before. For a typical human runner, the resultant orientation change in a single step is $\Delta\phi \lesssim 0.01$, negligibly small compared to the influence of the terrain. Thus, ignoring torques induced by gravity has minimal impact on our conclusions.

A finite stance duration and the associated change in configuration allows a runner to control the body’s sagittal plane angular momentum, independently from the forward and upward linear momenta. This may be understood in terms of breaking the symmetry of the stance phase or applying a large forward impulse and yet having the net ground reaction impulse pass through the center of mass (no contribution to angular momentum). To not lose such control when considering an impulse stance, we permit the application of an arbitrary angular impulse J_ϕ at the center of mass during push-off (equation (1c)). Thus having a finite stance duration and change of body configuration over stance is equivalent to J_{phi} (Fig. 8). The angular impulse also provides a means to

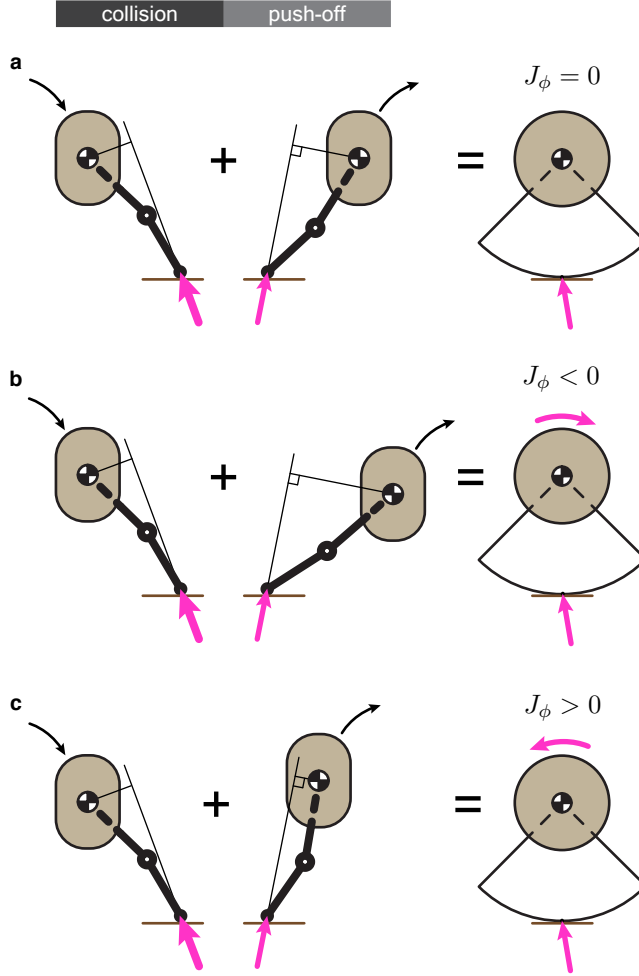


Figure 8: Equivalence between a runner using a freedom finite stance with internal degrees of freedom versus an infinitesimal stance with an applied torque impulse. The contact of the general runner is represented as an impulse due to the collision at touchdown (left, pink vector) plus a net impulse due to the push-off (right, pink vector). In this example, by varying duration of stance, the runner can selectively vary the lever arm of the push-off impulse and thus the angular impulse about its center of mass without altering the linear impulse. The net effect of a finite stance and change in configuration is therefore captured by a linear impulse at the point of contact (pink vector at ground) and an angular impulse at the center of mass (J_ϕ).

accommodate torques due to a finite base of support and a moving center of pressure during stance. However, recall that the constraint that the applied active push-off impulses should lead to perfectly periodic gait on flat terrain implies that $J_\phi = 0$. In our model, both open-loop and anticipatory runners slow down on rough terrain. Regaining forward speed needs a feedback controller, and then the additional control authority offered by J_ϕ would be necessary to vary forward speed without affecting the body's angular momentum or vertical momentum.

Point contact assumption

Another limitation arises from considering a point-like contact that cannot capture effects associated with the spatial extent of the foot. These effects include the spatial filtering of terrain roughness

and the application of a net torque about the initial contact point. The inclusion of J_ϕ in the model captures the application of torques, but there is no explicit means of incorporating the ability of the foot to act as a spatial filter (Venkadesan et al., 2017). Therefore, careful consideration should be given to the spatial frequency (wave number) of the roughness of the terrain when using a model with a point contact.

Timescale for feedback corrections

Open-loop runners with human-like parameters have a 99% chance of taking at least 3 steps without failing by exceeding the orientation threshold, while anticipatory runners ($\epsilon_{tc} = 1$) can take up to 15 steps with the same probability of completely losing forward momentum. This implies that the open-loop runner employing the slowest sensory modality (visual feedback delay ≈ 200 ms (van Beers et al., 2002)) has 7 feedback cycles to correct for instabilities at endurance running speeds of 3m/s (step period ≈ 500 ms (Cavagna et al., 1964)), with only an approximately 1% chance of an orientational failure. Thus, while sensory feedback is required to run on rough terrains, timescales associated with sensory feedback delays do not limit the runner’s ability to maintain stability because of the nature of the instability. Furthermore, employing an appropriate anticipatory strategy ($\epsilon_{tc} = 1$) eliminates the orientational instability entirely, thereby further extending the timescale over which feedback is necessary.

Leg retraction

Analyses of running models with leg mass suggest that optimal retraction rate is defined by stability demands, although these studies were limited to step-like terrains (Karssen et al., 2015). Experiments with runners on flat ground which measure the angle of the foot’s velocity vector with respect to the ground suggest that foot velocity is perhaps not modulated in the manner we hypothesize (Blum et al., 2010). In the study by Blum et al. (2010), the mean angle made by the subjects’ foot velocity vector with the ground was 165° , whereas our prediction based on zero tangential speed of the foot at touchdown would imply that the angle should be 90° . Given these differences, we propose that the low values of $\hat{\epsilon}_t$ for human runners observed by Dhawale and Venkadesan (2018) may result from joint stiffness modulation in the leg rather than precise control of the foot speed through leg retraction. Modulating foot and leg stiffness allows the runner to minimize the tangential collision and yet employ leg retraction strategies that accomplish other goals such as hypothesized by Seyfarth et al. (2003) and Birn-Jeffery et al. (2014).

Energy dissipation

Besides leg retraction, energy dissipation may also aid in stability based on studies of walking (Kuo, 1999; Donelan et al., 2001) and running (Daley et al., 2006; Arellano and Kram, 2011, 2012). Our model shows that while increasing energy dissipation in the direction normal to the terrain does increase the number of steps taken for open-loop and anticipatory runners, dissipating energy in the tangential collision is detrimental to stability. However, whether energy dissipation helps or hinders depends on the details of what is meant by “open-loop”. For example if the runner uses a *lab-fixed* push-off policy instead of the *terrain-fixed* push-off described in the main text, dissipating energy in the normal direction is also detrimental to orientational stability (supplement S9). Thus the hypothesized trade-off between energy consumption and stability is not universally true in our models. Our results are consistent with experiments on running birds encountering sudden terrain drops, as the birds do not always dissipate energy on the perturbation step (Daley et al., 2006). Our results might provide a means to understand why the increase in energy consumption for humans running on step-like terrains is only 5% (Voloshina and Ferris, 2015). We find that open-loop strategies are sufficient to maintain stability on step-like terrains and additional energy

expenditure provides little added benefit.

Implications of scaling analysis to body plan of animals

The single parameter $\phi_{\text{tol}}/\phi_{\bullet}$ that predicts mean steps to failure (Fig. 6) generalizes our results beyond runners with human-like parameters and can be used as a criteria to assess a runner’s stability. This is because runners with a larger $\phi_{\text{tol}}/\phi_{\bullet}$ should be able to maintain orientation for a greater number of steps in the absence of sensory feedback control. We have discussed how energy storage in the direction normal to the terrain (ϵ_n) and tangential collision modulation (ϵ_{tc}) affects $\phi_{\text{tol}}/\phi_{\bullet}$ in section 5, and now turn to the implications the parameter has on how body morphology and mass distribution affect stability.

The parameter ϕ_{tol} is the maximum angle of tilt the runner can accumulate before it falls. By employing larger (base/height) ratios, i.e. adopting a landscape rather than a portrait orientation when viewed in the sagittal plane, animals can increase ϕ_{tol} and thereby increase $\phi_{\text{tol}}/\phi_{\bullet}$. Quadrupeds such as cats and dogs, and other adept runners such as cockroaches possess such an aspect ratio. Another way to increase ϕ_{tol} is by increasing the range of motion of the leg with respect to the body. Even if the body begins to tilt, the ability to place the foot in front of the runner initiates stance and hence allows the runner to correct for body orientation. In our simulations, the choice of ϕ_{tol} value is based on this consideration of the leg angle for humans. Ostriches are another example of an animal with a portrait orientation but who are adept runners, perhaps in part due to the large of range of motion of their legs. Penguins, who are not known to be adept runners, occupy the opposite end of ϕ_{tol} scale due to possessing a portrait orientation and low range of motion of their legs compared to other bipeds such as humans, turkeys, and ostriches.

Because $\phi_{\text{tol}}/\phi_{\bullet} \propto I/G/v_{y0}^2$ (equations (12)), lowering take-off angles for a given forward speed would be beneficial to stability. However, very low take-off angles increase the risk of tripping on rough terrains. Altering body mass distribution to increase the radius of gyration r_g relative to leg length r_ℓ also reduces ϕ_{\bullet} and thereby increases stability. This can be achieved by increasing distal masses in appendages like arms and legs. However, increasing distal masses in the leg increases the metabolic cost of running (Myers and Steudel, 1985) via increased energetic cost associated with swinging the leg (Marsh et al., 2004; Doke et al., 2005) and may also lead to potentially injurious collisions. Alternatively, light legs with a bulky, extended torso or large head, like in horses and bison, also increases r_g . Lastly, tails in animals like cats and lizards, while used for active stabilization and in complex maneuvers like righting reflexes (Jusufi et al., 2011; Libby et al., 2012), are yet another means to increase r_g , thereby reducing ϕ_{\bullet} . Anticipatory runners further benefit from setting $\epsilon_t \approx 1$ like observed in humans (Dhawale and Venkadesan, 2018), thereby drastically reducing ϕ_{\bullet} as discussed in section 5. Thus, the dimensionless parameter $\phi_{\text{tol}}/\phi_{\bullet}$ is qualitatively consistent with the body morphology of adept and poor animal runners and we propose that it can be used as a design criteria for running robots.

7 Methods

7.1 Simulation methods

All simulations were performed using custom-written C programs. Parameter values given in table 1 are used for simulations of the human-like runner. These values are chosen for the purpose of illustration, however our qualitative results are not sensitive to these values, and the scaling analysis in section 5 addresses the generalization of these numerical results to runners and terrains with varying parameter values.

7.2 Parameter values for a human-like runner

The rationale for choosing the human-like parameter values is as follows. The moment of inertia value we use is derived from estimates made by (Erdmann, 1999), who find that moment of inertia about the center of mass in the sagittal plane is $\approx 13 \text{ kg}\cdot\text{m}^2$ for a 75 kg human. The value for $\epsilon_n = 0.63$ corresponds to $\approx 40\%$ elastic energy stored over one gait cycle, similar to estimates by (Cavagna et al., 1964; Cavagna and Kaneko, 1977; Alexander et al., 1987). The orientation bound ϕ_{tol} is equal to $\pi/6$ as it approximately half the angle between the legs during double stance in walking. Forward speed at take-off $v_{x0} = 0.96$ corresponds to 3 m/s for a leg length of 1 m and vertical speed at take-off $v_{y0} = 0.26$ corresponds to $\approx 0.8 \text{ m/s}$ (Dhawale and Venkadesan, 2018). Distributions had nearly converged by an ensemble size of 10^4 , hence we simulate for 10^5 instances (supplement S1).

7.3 Terrain model

The terrain is modelled as piecewise linear. This is achieved by first defining a one-dimensional grid with fixed grid spacing λ . Interpolating heights between the grid points k , located at x_k to intermediate points (x_t, y_t) in the k th terrain patch, yields a piecewise linear, continuous terrain profile, where terrain slope m_k is discontinuous at the grid points,

$$\text{patch } k : y_t = m_k x_t + c_k, \quad (16a)$$

$$\text{where } x_t \in [x_k, x_{k+1}], \quad (16b)$$

$$\text{continuity condition: } m_k x_{k+1} + c_k = m_{k+1} x_{k+1} + c_{k+1}, \quad (16c)$$

where m_k and c_k are constants within a patch. Terrain heights at all grid points are distributed according to $\sim \mathcal{U}(-0.03, 0.03)$ (table 1). Our choice of the uniform distribution \mathcal{U} is to improve simulation speed, even though beta distributions described in Fig. 2e most closely matched artificial terrain used in experiments (Dhawale et al., 2015; Dhawale and Venkadesan, 2018). The range of heights $h \in [-0.03, 0.03]$ and grid spacing $\lambda = 0.1$ was chosen to match the artificially constructed rough terrains (Dhawale et al., 2015; Dhawale and Venkadesan, 2018).

Step-like terrains with no slope distributions were simulated by picking a height from the probability distribution prior to landing. If the chosen landing height was above the apex height of any portion of the runner, we chose another landing height from the distribution. The probability of this resampling occurring is $\sim 10^{-4}$.

7.4 Calculating ground contact point

The aerial phase ends when the runner collides with the ground. The landing position is determined by solving for the unknown intersection point x_t of the runner's aerial phase trajectory (x_G, y_G) with the condition for tangential contact between runner and ground,

$$\text{parabolic flight: } y_G = b_0 + b_1 x_G + b_2 x_G^2, \quad (17a)$$

$$\text{touchdown: } y_G = y_t + \frac{1}{\sqrt{1 + m_k^2}}, \quad x_G = x_t - \frac{m_k}{\sqrt{1 + m_k^2}}, \quad (17b)$$

where b_0, b_1, b_2 are constants that define the aerial phase trajectory. Equations (16)-(17) solved simultaneously yield a quadratic equation in x_t ,

$$Ax_t^2 + Bx_t + C = 0, \quad (18a)$$

$$\text{where } A = b_2, \quad (18b)$$

$$B = b_1 - 2b_2 \frac{m_k}{\sqrt{1 + m_k^2}} - m_k, \quad (18c)$$

$$C = b_0 - \frac{b_1 m_k - 1}{\sqrt{1 + m_k^2}} + b_2 \frac{m_k^2}{1 + m_k^2} - c_k. \quad (18d)$$

The larger of the two roots of this quadratic is the true landing point x_P , if the roots are real and the larger of the two roots is greater than x_k . The other real root is always less than x_k and corresponds to the intersection of the aerial phase trajectory with the terrain patch closer to the take-off point. On flat terrain, the smaller root is the location of the take-off point. Having solved for x_P , the position of the center of mass at landing is determined using equation (17b).

However, if the runner lands on a grid point, the position of the center of mass appears to be indeterminate as the grid point x_k is associated with two slopes, m_k and m_{k+1} . In fact, we detect a corner collision if the larger root of equation (18a) is less than x_k , or if the roots are complex. Thus, we now know the position of contact point P, $x_P = x_k$, but cannot determine (x_G, y_G) at contact using equation (17b), since x_k is associated with slopes m_k and m_{k+1} . We determine a unique slope at the point x_k by accounting for the aerial phase trajectory. Substituting $x_t = x_k$ in equation (18a), we write equations (18) as a quartic polynomial in unknown m_k . We numerically find all the roots using the Jenkins-Traub algorithm (Jenkins and Traub, 1970) and pick the real root that corresponds to first contact between the ground and runner, i.e. when the parabolic trajectory describing the aerial phase is above the ground.

7.5 Notation

Scalars are denoted by italic symbols (e.g. m for mass of the runner, I for the moment of inertia), vectors by bold, italic symbols (\mathbf{J}_{imp} for push-off impulse, \mathbf{v} for velocity), points or landmarks in capitalized non-italic symbols (such as center of mass G in Fig. 1) and capitalized, bold, non-italic symbols for matrices (such as return map matrix \mathbf{T}_{an}). Vectors associated with a point, such as velocity of center of mass G are written as \mathbf{v}_G , with the uppercase alphabet in the subscript specifying the point in the plane. Angular momentum vectors or moment of inertia variables are subscripted with '/A' representing angular momentum or moment of inertia computed about point A, such as $I_{/G}$ representing moment of inertia about center of mass G. The component of velocity \mathbf{v}_A (velocity of point A) in the \hat{x} direction is denoted with a subscript 'A,t', e.g. tangential velocity of the contact point P is written as $v_{P,t}$. The symbols v_{x0}, v_{y0} denote the initial forward and vertical velocities of the runner at take-off. Variables just before collision with the terrain are denoted by the superscript '-', after passive collision but before push-off by the superscript 'c', and just after push-off by the superscript '+'. For example, angular velocity before collision is ω^- , after passive collision is ω^c and just after push-off is ω^+ .

8 Authors' Contribution

MV conceived of the model. ND and MV ran the simulations. All authors were involved in the analysis of the model; SM, MV and ND performed the linear stability analysis, MV and ND performed the one-step analysis to capture mean statistics, MV, SM and ND did the analysis of the steps to failure distributions. ND and MV wrote the manuscript, and all authors edited it.

9 Acknowledgments and funding

This work was funded by the Human Frontiers Science Program and the Wellcome/DBT India Alliance.

10 Competing interests

We have no competing interests.

References

- Alexander, R., Ker, R., Bennet, M., Bibby, S. and Kester, R. (1987). The spring in the arch of the human foot. *Nature* **325**, 147–149.
- Arellano, C. J. and Kram, R. (2011). The effects of step width and arm swing on energetic cost and lateral balance during running. *Journal of biomechanics* **44**, 1291–1295.
- Arellano, C. J. and Kram, R. (2012). The energetic cost of maintaining lateral balance during human running. *Journal of Applied Physiology* **112**, 427–434.
- Birn-Jeffery, A. V. and Daley, M. A. (2012). Birds achieve high robustness in uneven terrain through active control of landing conditions. *Journal of Experimental Biology* **215**, 2117–2127.
- Birn-Jeffery, A. V., Hubicki, C. M., Blum, Y., Renjewski, D., Hurst, J. W. and Daley, M. A. (2014). Don't break a leg: running birds from quail to ostrich prioritise leg safety and economy on uneven terrain. *Journal of Experimental Biology* **217**, 3786–3796.
- Blickhan, R. (1989). The spring-mass model for running and hopping. *Journal of biomechanics* **22**, 1217–1227.
- Blickhan, R. and Full, R. (1993). Similarity in multilegged locomotion: bouncing like a monopode. *Journal of Comparative Physiology A* **173**, 509–517.
- Blum, Y., Lipfert, S., Rummel, J. and Seyfarth, A. (2010). Swing leg control in human running. *Bioinspiration & biomimetics* **5**, 026006.
- Blum, Y., Vejdani, H. R., Birn-Jeffery, A. V., Hubicki, C. M., Hurst, J. W. and Daley, M. A. (2014). Swing-leg trajectory of running guinea fowl suggests task-level priority of force regulation rather than disturbance rejection. *PloS one* **9**, e100399.
- Bruijn, S., Meijer, O., Beek, P. and Van Dieën, J. (2013). Assessing the stability of human locomotion: a review of current measures. *Journal of the Royal Society Interface* **10**, 20120999.
- Byl, K. and Tedrake, R. (2009). Metastable walking machines. *The International Journal of Robotics Research* **28**, 1040–1064.
- Cavagna, G. and Kaneko, M. (1977). Mechanical work and efficiency in level walking and running. *The Journal of physiology* **268**, 467.
- Cavagna, G., Saibene, F. and Margaria, R. (1964). Mechanical work in running. *Journal of applied physiology* **19**, 249–256.
- Daley, M. A. and Usherwood, J. R. (2010). Two explanations for the compliant running paradox: reduced work of bouncing viscera and increased stability in uneven terrain. *Biology letters* **6**, 418–421.

- Daley, M. A., Usherwood, J. R., Felix, G. and Biewener, A. A.** (2006). Running over rough terrain: guinea fowl maintain dynamic stability despite a large unexpected change in substrate height. *Journal of Experimental Biology* **209**, 171–187.
- Dhawale, N., Mandre, S. and Venkadesan, M.** (2015). Running on rough terrains: Energetics and stability. *Dynamic Walking*.
- Dhawale, N. and Venkadesan, M.** (2018). Energetics and stability of running on rough terrains. American Society of Biomechanics.
- Dickinson, M. H., Farley, C. T., Full, R. J., Koehl, M., Kram, R. and Lehman, S.** (2000). How animals move: an integrative view. *Science* **288**, 100–106.
- Doke, J., Donelan, J. M. and Kuo, A. D.** (2005). Mechanics and energetics of swinging the human leg. *Journal of Experimental Biology* **208**, 439–445.
- Donelan, J. M., Kram, R. et al.** (2001). Mechanical and metabolic determinants of the preferred step width in human walking. *Proceedings of the Royal Society of London B: Biological Sciences* **268**, 1985–1992.
- Erdmann, W. S.** (1999). Geometry and inertia of the human body-review of research. *Acta of Bioengineering and biomechanics* **1**, 23–35.
- Full, R. J., Kubow, T., Schmitt, J., Holmes, P. and Koditschek, D.** (2002). Quantifying dynamic stability and maneuverability in legged locomotion. *Integrative and comparative biology* **42**, 149–157.
- Grimmer, S., Ernst, M., Günther, M. and Blickhan, R.** (2008). Running on uneven ground: leg adjustment to vertical steps and self-stability. *Journal of Experimental Biology* **211**, 2989–3000.
- Guckenheimer, J. and Holmes, P.** (1983). *Nonlinear oscillations, dynamical systems, and bifurcations of vector fields*. Springer-Verlag.
- Holmes, P., Full, R. J., Koditschek, D. and Guckenheimer, J.** (2006). The dynamics of legged locomotion: Models, analyses, and challenges. *Siam Review* **48**, 207–304.
- Jenkins, M. and Traub, J. F.** (1970). A three-stage algorithm for real polynomials using quadratic iteration. *SIAM Journal on Numerical Analysis* **7**, 545–566.
- Jusufi, A., Zeng, Y., Full, R. J. and Dudley, R.** (2011). Aerial righting reflexes in flightless animals.
- Karszen, J. D., Haberland, M., Wisse, M. and Kim, S.** (2015). The effects of swing-leg retraction on running performance: analysis, simulation, and experiment. *Robotica* **33**, 2137–2155.
- Kuo, A. D.** (1999). Stabilization of lateral motion in passive dynamic walking. *The International journal of robotics research* **18**, 917–930.
- Libby, T., Moore, T. Y., Chang-Siu, E., Li, D., Cohen, D. J., Jusufi, A. and Full, R. J.** (2012). Tail-assisted pitch control in lizards, robots and dinosaurs. *Nature* **481**, 181.

- Marsh, R. L., Ellerby, D. J., Carr, J. A., Henry, H. T. and Buchanan, C. I.** (2004). Partitioning the energetics of walking and running: swinging the limbs is expensive. *Science* **303**, 80–83.
- McGeer, T.** (1990). Passive bipedal running. *Proceedings of the Royal Society of London B: Biological Sciences* **240**, 107–134.
- McMahon, T. A. and Cheng, G. C.** (1990). The mechanics of running: how does stiffness couple with speed? *Journal of biomechanics* **23**, 65–78.
- Myers, M. and Steudel, K.** (1985). Effect of limb mass and its distribution on the energetic cost of running. *Journal of Experimental Biology* **116**, 363–373.
- Pearson, K.** (1993). Common principles of motor control in vertebrates and invertebrates. *Annual review of neuroscience* **16**, 265–297.
- Pearson, K. G.** (1995). Proprioceptive regulation of locomotion. *Current opinion in neurobiology* **5**, 786–791.
- Seyfarth, A., Geyer, H. and Herr, H.** (2003). Swing-leg retraction: a simple control model for stable running. *Journal of Experimental Biology* **206**, 2547–2555.
- Srinivasan, M. and Holmes, P.** (2008). How well can spring-mass-like telescoping leg models fit multi-pedal sagittal-plane locomotion data? *Journal of theoretical biology* **255**, 1–7.
- Srinivasan, M. and Ruina, A.** (2006). Computer optimization of a minimal biped model discovers walking and running. *Nature* **439**, 72–75.
- van Beers, R. J., Baraduc, P. and Wolpert, D. M.** (2002). Role of uncertainty in sensorimotor control. *Philosophical Transactions of the Royal Society B: Biological Sciences* **357**, 1137–1145.
- Venkadesan, M., Mandre, S. and Bandi, M. M.** (2017). *Bioinspired Legged Locomotion: Models, Concepts, Control and Applications, Chapter 7*. Butterworth-Heinemann.
- Voloshina, A. S. and Ferris, D. P.** (2015). Biomechanics and energetics of running on uneven terrain. *Journal of Experimental Biology* **218**, 711–719.
- Voloshina, A. S., Kuo, A. D., Daley, M. A. and Ferris, D. P.** (2013). Biomechanics and energetics of walking on uneven terrain. *Journal of Experimental Biology* **216**, 3963–3970.

Supplementary material for ‘How to run on rough terrains’

Nihav Dhawale, Shreyas Mandre and Madhusudhan Venkadesan

Contents

S1	Convergence of the Monte Carlo simulations	S2
S2	Model Details	S2
S2.1	Passive collision	S2
S2.2	Open-loop push-off strategies	S3
S3	Open-loop runners on rough terrain	S4
S3.1	The open-loop passive collision	S4
S3.2	Additive noise in open-loop strategies	S5
S4	Anticipatory runners on rough terrain	S6
S4.1	Forward collision parameter $\hat{\epsilon}_t$ as a function of ϵ_{tc}	S6
S5	Linear stability analysis: Jordan decomposition of T_{ol} and T_{an}	S7
S6	Scaling analysis of orientational failures	S9
S7	Steps to failure statistics	S11
S8	Effect of changing runner size relative to terrain grid spacing	S14
S9	Monte Carlo simulations with a <i>lab-fixed</i> push-off policy	S15
S9.1	Open-loop runners	S15
S9.2	Anticipatory runners	S16
S9.3	Scaling analysis of mean steps taken	S16

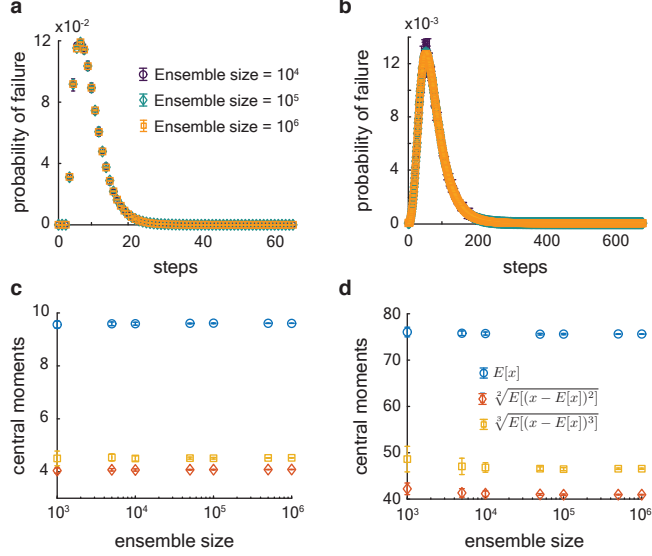


Figure S1: Monte Carlo simulations of open-loop and anticipatory runners with human-like parameter values and varying ensemble sizes. Ten simulations for each ensemble size were performed. Open markers represent the mean value, with error bars showing the standard deviation over the 10 runs. Steps to failure distributions for the **a**, open-loop runner and **b**, anticipatory runner. The y-axis of the plots is the joint probability $p(\text{falling at step number } i, \text{reaching step number } i)$. The first three central moments as a function of ensemble size for the **c**, open-loop runner and **d**, anticipatory runner are stationary for ensemble sizes greater than 10^4 .

S1 Convergence of the Monte Carlo simulations

We run Monte Carlo simulations with different ensemble sizes to test for convergence of the steps to failure distributions. Our criteria for convergence is met if the first three moments of the distribution are unchanged (one significant decimal place) as a function of ensemble size. This criteria is met with an ensemble size of 10^4 (Fig. S1). Hence we perform Monte Carlo simulations in the main text with an ensemble size of at least 10^5 .

S2 Model Details

S2.1 Passive collision

A runner with center of mass velocity \mathbf{v}_G^- and angular velocity ω^- , collides with a terrain patch angled at θ with respect to the horizontal. By simultaneously solving equations describing the collision at the contact point P (main text equation (1a)), and using kinematic constraints associated with a rigid body, the linear velocity \mathbf{v}_G^c and angular velocity ω^c of the runner after the collision

are computed as,

$$\text{collision law: } \mathbf{v}_P^c = \begin{pmatrix} \epsilon_t & 0 \\ 0 & -\epsilon_n \end{pmatrix} \mathbf{v}_P^-, \quad (\text{S1a})$$

$$H_{/P}^c - H_{/P}^- = 0, \quad (\text{S1b})$$

$$\text{kinematic constraint: } \mathbf{v}_G = \mathbf{v}_P - \omega \begin{pmatrix} \cos \theta \\ -\sin \theta \end{pmatrix}, \quad (\text{S1c})$$

$$\Rightarrow \mathbf{v}_G^c = \begin{pmatrix} \frac{(v_{G,x}^- \cos 2\theta + v_{G,y}^- \sin 2\theta)A + v_{G,x}^- B + C\omega^- \cos \theta}{2(I_G + 1)} \\ \frac{(v_{G,x}^- \sin 2\theta - v_{G,y}^- \cos 2\theta)A + v_{G,y}^- B + C\omega^- \sin \theta}{2(I_G + 1)} \end{pmatrix}, \quad (\text{S1d})$$

$$\text{and } \omega^c = \frac{(\epsilon_t + I_G)\omega^- - (1 - \epsilon_t)v_{G,t}^-}{1 + I_G}, \quad (\text{S1e})$$

$$\text{where } A = I_G(\epsilon_t + \epsilon_n) + \epsilon_n + 1, \quad B = \epsilon_t I_G - (I_G + 1)\epsilon_n + 1, \quad C = 2(\epsilon_t - 1)I_G, \quad (\text{S1f})$$

$$\text{and } v_{G,t} = v_{G,x} \cos \theta + v_{G,y} \sin \theta. \quad (\text{S1g})$$

S2.2 Open-loop push-off strategies

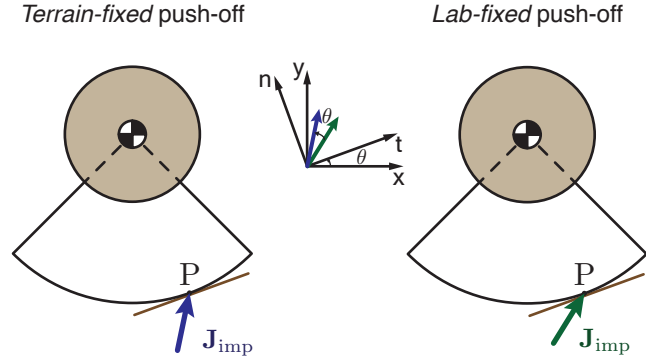


Figure S2: The *terrain-fixed* push-off impulse is the *lab-fixed* push-off impulse rotated by the terrain slope angle θ about the contact point.

After the passive collision, the push-off impulse \mathbf{J}_{imp} is applied at the contact point P to propel the runner into the flight phase. Recall that $J_\phi = 0$ for the open-loop push policies that we consider (main text equation (1c)). The push-off impulse \mathbf{J}_{imp} leads to discrete changes in the linear velocity of the center of mass \mathbf{v}_{imp} , and angular velocity of the runner ω_{imp} . As discussed in main text section 2.3, a *terrain-fixed* push-off policy or a *lab-fixed* push-off policy both satisfy the periodicity criteria on flat ground, namely $\mathbf{v}_{G,\text{steady}}^+ = (v_{x0}, v_{y0})^T$, and angular velocity is $\omega^+ = 0$, but differ in the effect on rough terrain. The linear velocity \mathbf{v}_G^+ and angular velocity ω^+ at take-off

under these push-off policies are,

$$\mathbf{v}_G^+ = \mathbf{v}_G^c + \mathbf{v}_{\text{imp}}, \quad \omega^+ = \omega^c + \omega_{\text{imp}}, \quad (\text{S2a})$$

$$\text{where } \mathbf{v}_{\text{imp}} = \begin{cases} \mathbf{R} \begin{pmatrix} \frac{I/G(1-\epsilon_t)v_{x0}}{I/G+1} \\ (1-\epsilon_n)v_{y0} \end{pmatrix} & : \textit{terrain-fixed}, \\ \begin{pmatrix} \frac{I/G(1-\epsilon_t)v_{x0}}{I/G+1} \\ (1-\epsilon_n)v_{y0} \end{pmatrix} & : \textit{lab-fixed}, \end{cases} \quad (\text{S2b})$$

$$\omega_{\text{imp}} = \begin{cases} \frac{(1-\epsilon_t)v_{x0}}{I/G+1} & : \textit{terrain-fixed}, \\ \frac{(1-\epsilon_t)v_{x0} \cos \theta}{I/G+1} + \frac{(1-\epsilon_n)v_{y0} \sin \theta}{I/G} & : \textit{lab-fixed}, \end{cases}, \quad (\text{S2c})$$

$$\text{and } \mathbf{R} = \begin{pmatrix} \cos \theta & -\sin \theta \\ \sin \theta & \cos \theta \end{pmatrix}, \quad (\text{S2d})$$

is the rotation matrix between the *lab-fixed* (x-y) reference frame and the *terrain-fixed* (t-n) reference frame (Fig. S2).

S3 Open-loop runners on rough terrain

S3.1 The open-loop passive collision

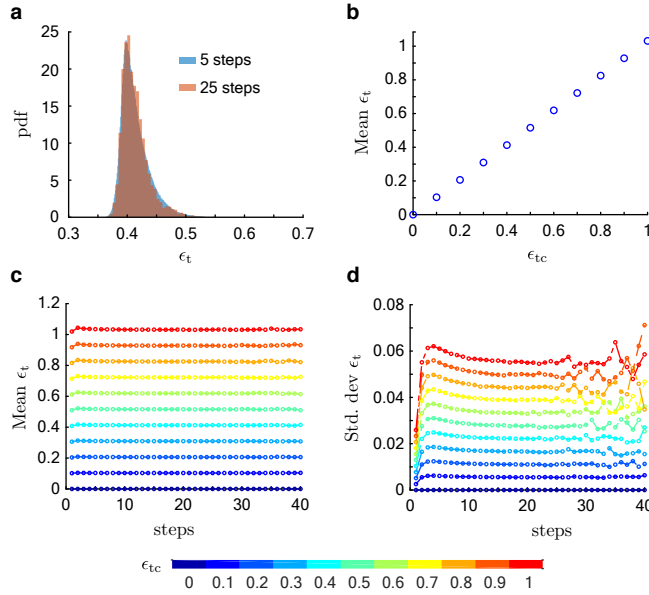


Figure S3: Tangential collisions in open-loop runners with human-like parameters on rough terrain. Monte Carlo simulations performed with 10^6 runners. **a**, The probability density function of ϵ_t after 5 steps and 25 steps for $\epsilon_{tc} = 0.4$. **b**, Steady-state mean ϵ_t increases linearly with ϵ_{tc} . **c**, Mean ϵ_t as a function of step number for different values of ϵ_{tc} (shown in the color bar below) converges by approximately 3 steps. **d**, Standard deviation of ϵ_t as a function of step number for different values of ϵ_{tc} also reaches a steady-state. However, the rate of convergence is slower at higher values of ϵ_{tc} . The fluctuations at higher step number ($\gtrsim 25$) are because we are probing the tails of the steps to failure distributions.

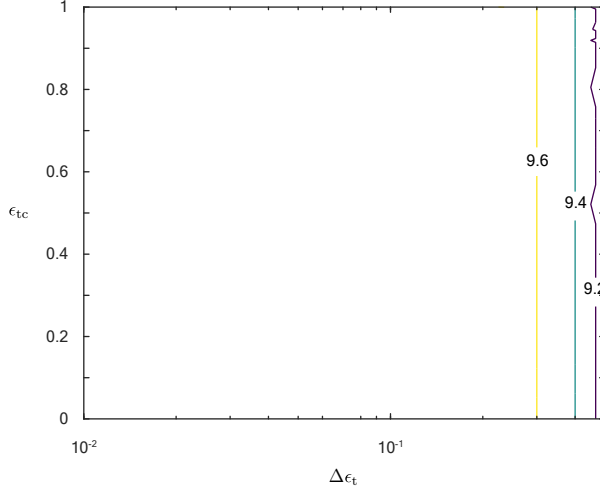


Figure S4: Effect of additive noise in ϵ_{tc} for open-loop runners with human-like parameters. Contour plot of mean steps to failure as a function of ϵ_{tc} and $\Delta\epsilon_t$. The mean steps to failure is constant as a function of ϵ_{tc} and $\Delta\epsilon_t$ below $\Delta\epsilon_t = 0.2$, and shows a small decrease with increasing $\Delta\epsilon_t$ when $\Delta\epsilon_t > 0.2$.

The tangential collision parameter ϵ_t for open-loop runners varies from step-to-step on rough terrains (main text equation (2)) and is thus characterized by distributions (Fig. S3a) that evolve according to running dynamics described in main text equation (1). These distributions achieve stationarity as seen in the representative case of the ϵ_t distribution with $\epsilon_{tc} = 0.4$, that appears to converge by 5 steps (Fig. S3a). Mean ϵ_t converges by 3 steps to values that are just a little larger than the corresponding ϵ_{tc} values (Fig. S3c), and show a linear dependence on ϵ_{tc} (Fig. S3b). The shape of the distribution is affected by the ϵ_{tc} value as the standard deviation of the converged ϵ_t distribution increases with ϵ_{tc} (Fig. S3d).

The stability benefits of higher mean ϵ_t values (Fig. S3b) are counteracted by corresponding higher fluctuations in ϵ_t (Fig. S3d), leading to larger step-to-step fluctuations in body angular momentum. Hence for open-loop runners, mean steps to failure shows a weak dependence on ϵ_{tc} value. In main text section 5, we arrive at this same conclusion via an asymptotic analysis of the series expansion of the orientation change over a single step caused by an unexpected terrain slope perturbation.

S3.2 Additive noise in open-loop strategies

Additive noise in the tangential collision (main text section 3.5) of open-loop runners has little effect on mean steps to failure (Fig. S4) compared to the same noise intensity applied to anticipatory runners (main text Fig. 3b). For open-loop runners with human-like parameters, there is no optimal value of ϵ_{tc} (Fig. S4) unlike the case with anticipatory runners where slight tangential collisions are optimal (main text Fig. 3b). The relative insensitivity of failure statistics to added noise for the open-loop runner is possibly because ϵ_t varies significantly on rough terrains even in the absence of added noise (Fig. S3).

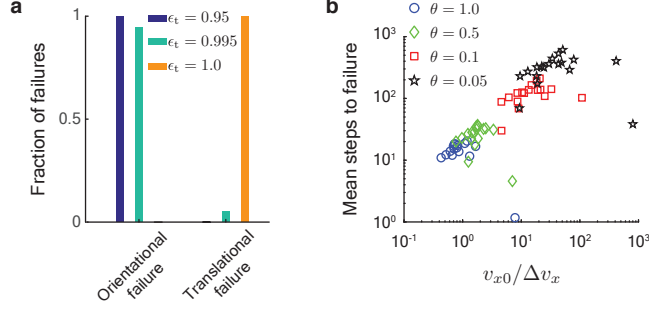


Figure S5: Anticipatory runners on rough terrain. **a**, Relative frequency of failure modes for anticipatory runners with $\epsilon_n = 0$ on rough terrain. The orientation failure bound $\phi_{\text{tol}} = \pi/6$ in these simulations and other parameters are the same as those for the human-like runner (main text table 1) **b**, Mean steps to failure as function of $v_{x0}/\Delta v_x$ for the same range of parameters shown in Fig. S7, except that $\epsilon_{tc} = 1$ here.

S4 Anticipatory runners on rough terrain

In main text section 3.4 we describe how zeroing the tangential collision impulse stabilizes orientation, but deviations from this strategy quickly leads to a loss in stability. To underscore how quickly failure modes change, consider that anticipatory runners with $\epsilon_{tc} = 1$ fail exclusively due to translational instabilities while anticipatory runners with human-like parameters and $\epsilon_{tc} = 0.95$ fail exclusively due to orientational instabilities (Fig. S5a). Thus, the predominant failure mode switches quickly from translational failures to orientation failures close to $\epsilon_{tc} = 1$; even runners with $\epsilon_{tc} = 0.995$ predominantly undergoing orientational failures (Fig. S5a).

The mean steps to failure for an anticipatory runner with $\epsilon_{tc} = 1$ is captured by a single parameter $v_{x0}/\Delta v_x$ (Fig. S5b). The logic is similar to that in main text section 5 where the scaling analysis is for orientational failures, while here the failure mode is due to losing translational stability (main text Fig. 1c). For a runner landing on sloped ground with forward speed $v_{G,x}^- = v_{x0}$, the loss in forward speed due to the terrain perturbation is $\Delta v_x = v_{x0} - v_{G,x}^+$ over a single step. Following the logic outlined in main text section 5, the mean steps to failure N should scale as,

$$N \sim v_{x0}/\Delta v_x, \quad (\text{S3a})$$

$$\text{where } \Delta v_x = \sin \theta (v_{y0} (\cos \theta - 1 + \epsilon_n (\cos \theta + 1)) + v_{x0} \sin \theta (1 + \epsilon_n)). \quad (\text{S3b})$$

$$\text{Power series: } \Delta v_x = 2\epsilon_n v_{y0} \theta + v_{x0} (1 + \epsilon_n) \theta^2 + O(\theta^3). \quad (\text{S3c})$$

Equation (S3c) is the power series expansion for Δv_x about $\theta = 0$ to second order in θ . The power series analysis suggests that shallower flight trajectories (reducing v_{y0}) and increasing energy dissipation (reducing ϵ_n) increases the mean steps to translational failure. Results from the Monte Carlo simulations in main text Fig. 3a find that reducing ϵ_n increases mean steps taken for anticipatory runners with $\epsilon_{tc} = 1$, consistent with equations (S3b)-(S3c).

S4.1 Forward collision parameter $\hat{\epsilon}_t$ as a function of ϵ_{tc}

The forward collision parameter $\hat{\epsilon}_t$ is characterized by a distribution as described in main text section 3.6. The distributions of $\hat{\epsilon}_t$ with $\epsilon_{tc} = 0.5$ after 3 steps and 20 steps are relatively unchanged (Fig. S6a) in comparison to the distribution of $\hat{\epsilon}_t$ with $\epsilon_{tc} = 1$ (main text Fig. 4a) where the distribution broadens significantly more. The mean of the distribution for all values of ϵ_{tc} converges by

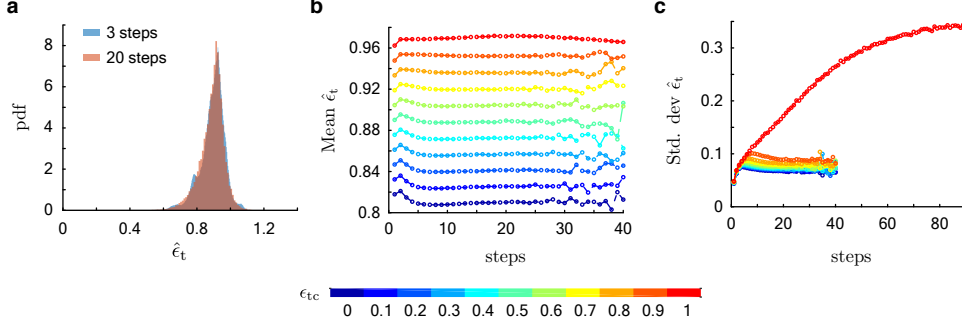


Figure S6: Evolution of forward collision parameter $\hat{\epsilon}_t$ as a function of step number and ϵ_{tc} . **a**, The probability density function of $\hat{\epsilon}_t$ after 3 steps and 20 steps for $\epsilon_{tc} = 0.5$. **b**, Mean $\hat{\epsilon}_t$ as a function of step number for different values of ϵ_{tc} (shown in the color bar below). The mean converges by approximately 5 steps for all values of ϵ_{tc} . **c**, Standard deviation of $\hat{\epsilon}_t$ as a function of step number for different values of ϵ_{tc} . While the standard deviation converges by 15 steps for values of $\epsilon_{tc} < 1$, for $\epsilon_{tc} = 1$ it increases monotonically, plateauing only after approximately 80 steps.

5 steps (Fig. S6b), while the standard deviation for ϵ_{tc} sufficiently below 1 converges by approximately 15 steps (Fig. S6c). When $\epsilon_{tc} = 1$, or if ϵ_{tc} is sufficiently close to 1, the standard deviation of the distribution approaches steady state only after 80 steps.

S5 Linear stability analysis: Jordan decomposition of \mathbf{T}_{ol} and \mathbf{T}_{an}

The linear stability analysis for the open-loop runner proceeds analogously to the analysis for the anticipatory runner discussed in main text section 4. We define a Poincaré section transverse to the runner's trajectory in phase space at the apex of the aerial phase ($v_y = 0$), and a return map f_{ol} that maps the state of the runner ψ_n at the apex of the aerial phase at step n , to the state at the apex of the aerial phase on the following step ψ_{n+1} (main text Fig. 5). The state ψ , return map f_{ol} , and its linearization \mathbf{T}_{ol} are defined by,

$$\psi = (x \ y \ \phi \ v_x \ \omega)^T \quad (\text{S4a})$$

$$\psi_{n+1} = f_{ol}(\psi_n), \quad (\text{S4b})$$

$$\Delta\psi_{n+1} = \mathbf{T}_{ol}\Delta\psi_n, \text{ where } \mathbf{T}_{ol} = \left. \frac{\partial f_{ol}}{\partial \psi} \right|_{\psi^*}, \quad (\text{S4c})$$

$$\text{and } \Delta\psi = \psi - \psi^*, \text{ where } \psi^* = f_{ol}(\psi^*). \quad (\text{S4d})$$

The linearized return maps, \mathbf{T}_{ol} and \mathbf{T}_{an} are non-diagonalizable as discussed in main text section 4. Thus an eigen-factorization of these matrices is not possible, so we perform a Jordan decomposition

decomposition of \mathbf{T}_{an} when $\epsilon_{\text{tc}} < 1$ is,

$$\mathbf{T}_{\text{an}} = \mathbf{V}_{\text{an}} \mathbf{J}_{\text{an}} \mathbf{V}_{\text{an}}^{-1}, \quad (\text{S7a})$$

$$\text{where } \mathbf{J}_{\text{an}} = \begin{pmatrix} 1 & 0 & \sqrt{2}\epsilon_n v_{y0} & 0 & 0 \\ 0 & 1 & -\sqrt{2}\epsilon_n v_{y0} & 0 & 0 \\ 0 & 0 & 1 & 0 & 0 \\ 0 & 0 & 0 & \epsilon_n(2\epsilon_n - 1) & 0 \\ 0 & 0 & 0 & 0 & \epsilon_t \end{pmatrix}, \quad (\text{S7b})$$

$$\text{and } \mathbf{V}_{\text{an}} = \begin{pmatrix} 0 & 1 & 0 & 0 & \frac{(1+\epsilon_t(2\epsilon_n-1))I/G v_{y0}}{\epsilon_t-1} \\ 0 & 0 & 0 & 1 & 0 \\ 1 & 0 & 0 & 0 & \frac{(1+\epsilon_t(2\epsilon_n-1))v_{y0}}{\epsilon_t-1} \\ 0 & 0 & \frac{-1}{\sqrt{2}} & 0 & I/G \\ 0 & 0 & \frac{1}{\sqrt{2}} & 0 & 1 \end{pmatrix}. \quad (\text{S7c})$$

The anticipatory runner has a full rank return map \mathbf{T}_{an} , and stable eigenvalues $\lambda = \epsilon_n(2\epsilon_n - 1)$, which is identical to the open-loop runner, and $\lambda = \epsilon_t$ which differs from the open-loop runner. The off-diagonal elements of \mathbf{J}_{an} are $a_1 = \sqrt{2}\epsilon_n v_{y0}$ and $a_2 = -\sqrt{2}\epsilon_n v_{y0}$ (equation S7b), which correspond to the projection onto $\boldsymbol{\nu}_1$ and $\boldsymbol{\nu}_2$ respectively, of a perturbation along $\boldsymbol{\nu}_3$ upon action of the return map \mathbf{T}_{an} .

When $\epsilon_{\text{tc}} = \epsilon_t = 1$ for the anticipatory runner, the linearization of \mathbf{f}_{an} about $\boldsymbol{\psi}^*$ (main text equations 7) yields a different form for \mathbf{T}_{an} . The Jordan decomposition of \mathbf{T}_{an} when $\epsilon_{\text{tc}} = 1$ is,

$$\mathbf{T}_{\text{an}} = \mathbf{V}_{\text{an}} \mathbf{J}_{\text{an}} \mathbf{V}_{\text{an}}^{-1}, \quad (\text{S8a})$$

$$\text{where } \mathbf{J}_{\text{an}} = \begin{pmatrix} 1 & 2\epsilon_n v_{y0} & 0 & 0 & 0 \\ 0 & 1 & 0 & 0 & 0 \\ 0 & 0 & 1 & 2\epsilon_n v_{y0} & 0 \\ 0 & 0 & 0 & 1 & 0 \\ 0 & 0 & 0 & 0 & \epsilon_n(2\epsilon_n - 1) \end{pmatrix}, \quad (\text{S8b})$$

$$\text{and } \mathbf{V}_{\text{an}} = \begin{pmatrix} 0 & 0 & 1 & 0 & 0 \\ 0 & 0 & 0 & 0 & 1 \\ 1 & 0 & 0 & 0 & 0 \\ 0 & 0 & 0 & 1 & 0 \\ 0 & 1 & 0 & 0 & 0 \end{pmatrix}. \quad (\text{S8c})$$

There is a single stable eigenvalue of $\lambda = \epsilon_n(2\epsilon_n - 1)$ which is identical to that of the open-loop runner and the anticipatory runner with $\epsilon_{\text{tc}} < 1$. The remaining 4 eigenvalues are $\lambda = 1$ which are associated with eigenvectors $\boldsymbol{\nu}_1$, $\boldsymbol{\nu}_2$ and generalized eigenvectors $\boldsymbol{\nu}_3$ and $\boldsymbol{\nu}_4$ (main text equations (10a)). Perturbations along $\boldsymbol{\nu}_3$ project onto $\boldsymbol{\nu}_1$, and perturbations along $\boldsymbol{\nu}_4$ project onto $\boldsymbol{\nu}_2$, upon action of the return map \mathbf{T}_{an} (equation (S8b)). The off-diagonal elements of \mathbf{J}_{an} are $a_1 = a_2 = 2\epsilon_n v_{y0}$.

S6 Scaling analysis of orientational failures

In main text section 5, we show that the orientation failure bound ϕ_{tol} and the orientation change over a single step ϕ_{\bullet} from encountering an unexpected terrain slope predict the mean steps to failure N , as $N \sim \phi_{\text{tol}}/\phi_{\bullet}$. The many parameters that define the runner and its gait do not separately

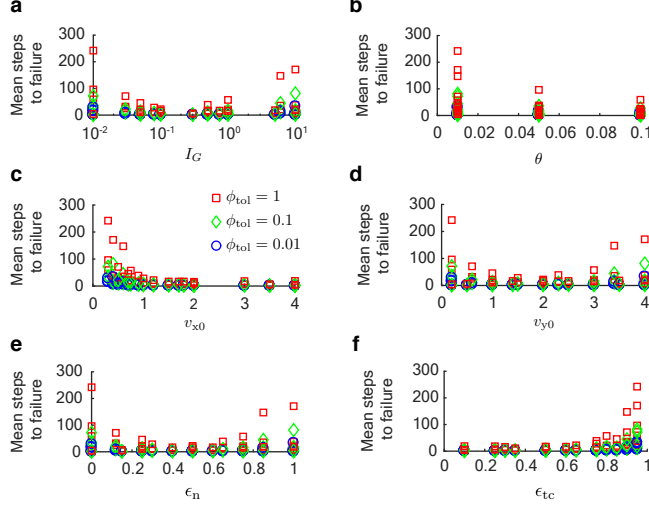


Figure S7: Mean steps to failure for the anticipatory runner ($\epsilon_{tc} < 1$) plotted against all other parameters: I/G , θ , v_{y0} , ϵ_n , v_{x0} , ϵ_{tc} . Here, θ refers to the typical slope angle the runner would encounter, defined as $\theta = h/\lambda$, where λ is the grid spacing of the terrain and $[-h, h]$ is the range of heights of the terrain (main text section 7.3).

predict mean steps to failure as accurately as the parameter $\phi_{tol}/\phi_{\bullet}$ (Fig. S7).

The change in orientation over one step can be calculated using the vertical velocity $v_{y,\bullet}^+$ and angular velocity ω_{\bullet}^+ at take-off as $\phi_{\bullet} = 2v_{y,\bullet}^+ \omega_{\bullet}^+$ ($\bullet = \text{'ol'}$ for open-loop and 'an' for anticipatory). For a runner landing on a terrain patch angled at θ with respect to the horizontal, with center of mass velocity $\mathbf{v}_G^- = (v_{x0} \quad -v_{y0})^T$ and angular velocity $\omega^- = 0$, the take-off velocities $v_{y,\bullet}^+$, ω_{\bullet}^+ , and orientation change ϕ_{\bullet} , are given by

$$\omega_{an}^+ = \frac{(1 - \epsilon_{tc})(v_{x0}(1 - \cos \theta) + v_{y0} \sin \theta)}{1 + I/G}, \quad (\text{S9a})$$

$$\omega_{ol}^+ = \frac{v_{x0}(1 - \cos \theta) + v_{y0} \sin \theta}{1 + I/G}, \quad (\text{S9b})$$

$$v_{y,an}^+ = v_{y0} + \frac{(1 + \epsilon_n + I/G\epsilon_n)(v_{x0} \sin 2\theta - v_{y0}(1 - \cos 2\theta))}{2(1 + I/G)}, \quad (\text{S9c})$$

$$v_{y,ol}^+ = v_{y,an}^+ + \frac{2\epsilon_{tc}v_{x0} \sin \theta}{2(1 + I/G)}, \quad (\text{S9d})$$

$$\phi_{an} = \frac{1 - \epsilon_{tc}}{(1 + I/G)^2} A(B + (\epsilon_{tc} - 1)C + (D + I/G\epsilon_{tc})E + F - I/G\epsilon_{tc}v_{y0}),$$

$$\phi_{ol} = \frac{1}{(1 + I/G)^2} A(B + (2\epsilon_{tc} - 1)C + DE + F), \quad (\text{S9e})$$

where $A = v_{y0} \sin \theta + v_{x0}(1 - \cos \theta)$, $B = 2(1 + I/G)(1 - \epsilon_n)v_{y0} \cos \theta$,

$$C = 2I/Gv_{x0} \sin \theta, \quad D = 1 + \epsilon_n + I/G\epsilon_n,$$

$$E = v_{y0} \cos 2\theta + v_{x0} \sin 2\theta, \quad F = (I/G\epsilon_n + \epsilon_n - 1)v_{y0}.$$

The parametric dependence of $\phi_{tol}/\phi_{\bullet}$ (ϕ_{\bullet} defined in equation (S9e)) on ϵ_{tc} and ϵ_n is captured by a power series approximation of ϕ_{\bullet} to second order in θ (main text equations (12a)-(12b)). The

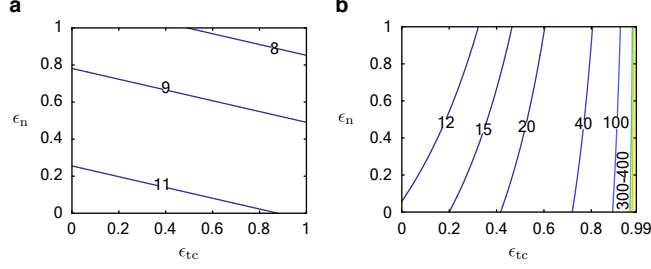


Figure S8: Contour plots of **a**, $\phi_{\text{tol}}/\phi_{\text{ol}}$ and **b**, $\phi_{\text{tol}}/\phi_{\text{an}}$ as a function of ϵ_n and ϵ_{tc} , where the form of ϕ_{\bullet} shown in the power series expansion to second order in θ has been used (main text equations (12a)-(12b)). The values of the contours differ slightly between the plots shown here and in the main text Fig. 7 but the qualitative trends are the same. The same parameter values are used in both these calculation, $v_{y0} = 0.2, I/G = 0.15, v_{x0} = 1, \theta = 0.3, \phi_{\text{tol}} = 1$. For the anticipatory runner, maximum $\epsilon_{\text{tc}} = 0.99$ to ensure that the calculation is limited to the region where runners primarily undergo orientational failures (Fig. S5a).

contour plots of $\phi_{\text{tol}}/\phi_{\bullet}$ shown here using the truncated power series form of ϕ_{\bullet} (Fig. S8) display the same qualitative trends as the ones in main text Fig. 7 which use the complete expression for ϕ_{\bullet} (equation (S9e)). Therefore, we analyze failure statistics and runner morphology in main text section 5 and section 6 using the truncated power series approximation for ϕ_{\bullet} .

S7 Steps to failure statistics

All steps to failure distributions show similar qualitative features; they are unimodal with a long tail, and are relatively insensitive to changes in the terrain height distribution (Fig. S1, main text Fig. 2e). This suggests that the stochastic dynamics underlying these distributions are characterized by a small number of parameters that govern angular momentum fluctuations of the runner, as most runners fail by losing orientational stability.

To arrive at this lower-order model, we start with the result from the linear stability analysis of the runner which states that the orientation of the runner ϕ grows linearly with step number n in response to small perturbations to the periodic orbit (main text section 4). A second-order difference equation that displays linear growth in step number n of an initial perturbation $\phi(1) - \phi(0)$ is,

$$\phi(n+2) = 2\phi(n+1) - \phi(n), \quad (\text{S10a})$$

$$\implies \phi(n) = n(\phi(1) - \phi(0)) + \phi(0). \quad (\text{S10b})$$

For the runner, perturbations arise from terrain slope variations and are thus stochastic in nature. Thus, we incorporate stochasticity in this model using an additive noise term,

$$\phi(n+2) = 2\phi(n+1) - \phi(n) + w, \quad (\text{S11a})$$

$$\text{where } w \sim N(0, \sigma^2), \quad (\text{S11b})$$

and $N(0, \sigma^2)$ is the normal distribution with mean = 0 and standard deviation = σ . We assume that after a sufficiently large number of steps, $\phi(n)$ would have Gaussian statistics as terrain perturbations are uncorrelated from step-to-step. This invocation of the mean value theorem, while not rigorous, is done primarily to simplify the analysis. With initial conditions $\phi(1) = \phi(0) = 0$,

the probability distribution of ϕ after n steps is given by

$$p(\phi, n) = \frac{e^{-\frac{\phi^2}{2\sigma^2 f(n)}}}{\sqrt{2\pi\sigma^2 f(n)}}, \quad (\text{S12a})$$

$$\text{where } f(n) = \frac{n(n+1)(2n+1)}{6} \quad (\text{S12b})$$

$$\text{and } f(n) \sim \frac{n^3}{3}, \text{ for } n \gg 1. \quad (\text{S12c})$$

The probability distribution $p(\phi, n)$ is Gaussian with $\langle \phi \rangle = 0$ and variance that grows as n^3 for large n .

Orientation failures occur when a runner's orientation exceeds ϕ_{tol} . Thus, the probability of having failed by n steps, which we denote with $p_{\text{fall}}(n)$, is given by

$$p_{\text{fall}}(n) = p(|\phi| > \phi_{\text{tol}}, n), \quad (\text{S13a})$$

$$\implies p_{\text{fall}}(n) = 1 - \text{erf}\left(\frac{\phi_{\text{tol}}}{\sqrt{2\sigma^2 f(n)}}\right), \quad (\text{S13b})$$

$$\text{where } \text{erf}(x) = \frac{1}{\sqrt{\pi}} \int_{-x}^x e^{-u^2} du, \quad (\text{S13c})$$

is the error function. The probability of failing at step number n , denoted by $p_{\text{steps}}(n)$, is given by the probability of taking $n-1$ steps without failing, and then failing at step number n , i.e. $p_{\text{steps}}(n) = p(|\phi| > \phi_{\text{tol}}, n \mid |\phi| < \phi_{\text{tol}}, n-1)$. This is equivalent to the probability flux at ϕ_{tol} at step n , given by

$$p_{\text{steps}}(n) = p_{\text{fall}}(n) - p_{\text{fall}}(n-1), \quad (\text{S14a})$$

$$\implies p_{\text{steps}}(n) = \text{erf}\left(\frac{\phi_{\text{tol}}}{\sqrt{2\sigma^2 f(n-1)}}\right) - \text{erf}\left(\frac{\phi_{\text{tol}}}{\sqrt{2\sigma^2 f(n)}}\right). \quad (\text{S14b})$$

The mean steps to failure M are thus given by

$$M = \sum_{n=0}^{\infty} n p_{\text{steps}}(n), \quad (\text{S15a})$$

$$\implies M = \sqrt{\frac{6}{\pi}} \sum_{i=1}^{\infty} -1^{i+1} \left(\frac{3}{2}\right)^i \zeta\left(\frac{3(2i-1)}{2}\right) \frac{(\phi_{\text{tol}}/\sigma)^{2i-1}}{(i-1)!}, \quad (\text{S15b})$$

$$\text{where we have used } f(n) \approx \frac{n^3}{3}, \quad (\text{S15c})$$

and $\zeta(p)$ is the Riemann-zeta function defined by $\zeta(p) = \sum_{i=0}^{\infty} 1/i^p$ for $p > 1$.

The probability of failing at step n , $p_{\text{steps}}(n)$ (Fig. S9a), and its cumulative distribution $p_{\text{fall}}(n)$ (Fig. S9b) are qualitatively similar to the numerically derived steps to failure distributions shown in Fig. S1 and main text Fig. 2e, and the cumulative distributions shown in main text Fig. 2a,b.

Interpreting the standard deviation of the noise from the terrain as $\sigma = \phi_{\bullet}$, since ϕ_{\bullet} sets the scale for orientation change over a single step due to an unexpected terrain slope (main text section 5), we do not find quantitative agreement between our stochastic model and the numerics. The mean

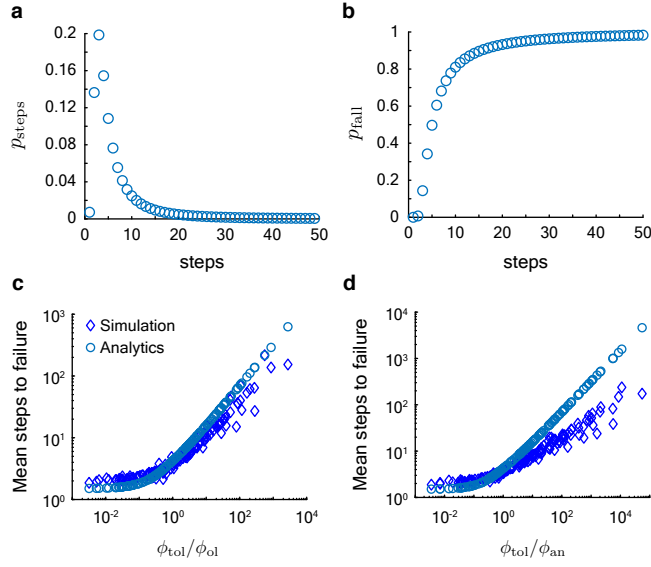


Figure S9: Steps to failure statistics of the single parameter stochastic model. **a**, p_{steps} from equation (S14) and **b**, p_{fail} from equation (S13) plotted against steps taken n with human-like parameter values for ϕ_{tol} and $\sigma = \phi_{\text{ol}}$ (main text table 1). The mean of this distribution 9.6, is remarkably similar to the numerical mean steps to failure for the open-loop runner with human-like parameters which is 9.61 ± 0.01 . However, for a wider range of $\phi_{\text{tol}}/\phi_{\bullet}$ values, the mean of the analytical model (open circles) for **c**, open-loop runners and **d**, anticipatory runners deviates from mean steps to failure from the Monte Carlo simulations (open diamonds, main text Fig. 6). The parameters values used for ϕ_{tol} and ϕ_{\bullet} are shown in Fig. S7.

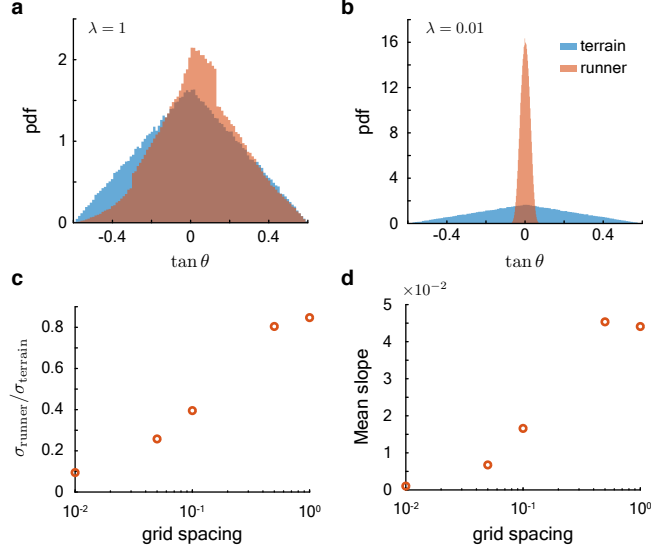


Figure S10: Effect of varying the ratio of leg length r_ℓ to terrain grid spacing λ . The probability density function of the terrain slope ($\tan \theta$) encountered by the open-loop runner (orange) with human-like parameters is plotted for grid spacing **a**, $\lambda = r_\ell$ and **b**, $\lambda = 0.01r_\ell$. The height distribution of the terrain grid points was adjusted so that the terrain’s slope distribution (blue) was the same in all simulations. The number of steps used to generate these probability density functions was $\sim 10^6$. **c**, Shows the standard deviation of the slope encountered by the runner relative to the standard deviation of the terrain’s slope distribution. **d**, The mean slope encountered by the runner is always positive and increases with grid spacing, even though the terrain’s slope distribution is held constant.

of the analytical distribution (equation (S15b)) has a different power law scaling compared to mean steps to failure obtained from the Monte Carlo simulations (Fig. S9c,d).

S8 Effect of changing runner size relative to terrain grid spacing

The size of the runner r_ℓ , relative to the grid spacing of the terrain λ , determines the range of terrain slopes accessed by the runner (main text section 6, Fig. S10). For example, if $\lambda/r_\ell = 1$, the range of terrain slopes encountered by the runner is nearly the same as the slope distribution of the terrain itself (Fig. S10a). By decreasing this ratio to $\lambda/r_\ell = 0.01$ while keeping the terrain slope distribution constant, we find that the range of slopes encountered by the runner is significantly lower (Fig. S10b). We quantify this trend using the parameter $\sigma_{\text{runner}}/\sigma_{\text{terrain}}$ where σ_{terrain} is the standard deviation of the terrain slope distribution, and σ_{runner} is the standard deviation of the slope distribution encountered by the runner. The parameter $\sigma_{\text{runner}}/\sigma_{\text{terrain}}$ approaches 1 as λ/r_ℓ increases (Fig. S10c).

The mean slope encountered by the runner is always greater than zero (Fig. S10d) even though the slope distribution of the terrain has a zero mean. As the range of slopes encountered by the runner increases, the mean slope encountered by the runner deviates further from zero (Fig. S10d). This is consistent with the observation from the Monte Carlo simulations that runners slow down on rough terrain since the effect of the mean slope encountered is to redirect forward momentum into vertical momentum.

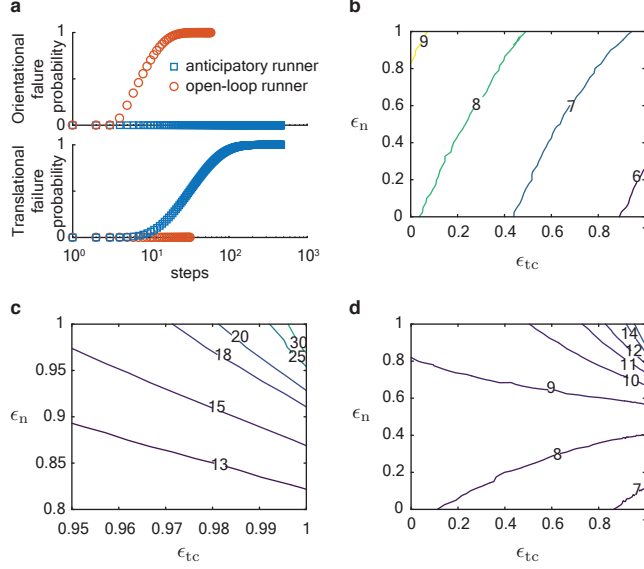


Figure S11: Runners with a *lab-fixed* push-off policy: effect of energy dissipation and tangential collisions. **a**, Open-loop runners with human-like parameters and $\epsilon_{tc} = 0, \epsilon_n = 1$ undergo orientational failures on rough terrain while human-like anticipatory runners with $\epsilon_{tc} = 1, \epsilon_n = 1$ maintain orientation but lose forward momentum. **b**, Contour map of mean steps to failure for the human-like open-loop runner as a function of ϵ_n and ϵ_{tc} . **c**, Contour map of the mean steps to failure for the anticipatory runner as a function of ϵ_n and ϵ_{tc} , zoomed into the region near the maximum steps taken, where contour spacing is small. **d**, Away from the maximum, contour spacing increases for the anticipatory runner, demonstrating reduced sensitivity to changes in ϵ_n and ϵ_{tc} . The $\epsilon_{tc} = 0$ strategy is identical between the open-loop and anticipatory runners like with the *terrain-fixed* push-off policy.

S9 Monte Carlo simulations with a *lab-fixed* push-off policy

The change in angular velocity due to the push-off impulse \mathbf{J}_{imp} applied under the *lab-fixed* push-off policy is terrain dependent and destabilizes the runner as it exacerbates angular momentum fluctuations that arise from variations in terrain slope angle θ . When $\theta > 0$, the runner collides with lower tangential velocity as compared to landing on flat ground, yet the change in angular velocity at push-off ω_{imp} , is larger than the corresponding impulse on flat ground (equation S2d) causing the runner to spin excessively in the anti-clockwise direction. Conversely, when $\theta < 0$, the runner lands at a shallower angle, increasing the tangential collision impulse. The change in angular velocity ω_{imp} is lower than on flat ground (equation S2d), causing the runner to spin in the clockwise direction. In contrast, ω_{imp} under the *terrain-fixed* push-off policy is unchanged by terrain slope θ (equation S2d) and thus, in all cases, the *lab-fixed* push-off policy leads to a lower number of steps taken compared to the *terrain-fixed* push-off policy.

S9.1 Open-loop runners

Increasing energy dissipation in the direction normal to the terrain surface reduces mean steps taken by open-loop runners with a *lab-fixed* push-off policy in contrast to the trend observed with the *terrain-fixed* push-off where increasing normal energy dissipation, nominally increased steps taken (main text Fig. 2d). With the *lab-fixed* push-off, open-loop runners with human-like parameters

only fail due to losing orientational stability (Fig. S11a) and increase mean steps taken by at most 1 for a 100% reduction in energy dissipation from $\epsilon_n = 0$ to $\epsilon_n = 1$ at a fixed value of ϵ_{tc} (Fig. S11b).

Reducing tangential collisions increases steps taken (Fig. S11b), in contrast to the trend observed with the *terrain-fixed* push-off strategy where changing ϵ_{tc} had negligible effect on the mean steps to failure (main text Fig. 2d). Open-loop runners increase mean steps taken by 2 when ϵ_{tc} is reduced from 1 to 0, while holding ϵ_n fixed at any value (Fig. S11b).

Open-loop runners with a *lab-fixed* push-off policy perform best when $\epsilon_n = 1, \epsilon_{tc} = 0$ and worst when $\epsilon_n = 0, \epsilon_{tc} = 1$. The difference in mean steps taken at these extremes is just 3 steps, with the maximum of 9 steps being the same as the minimum number of steps taken by human-like open-loop runners with the *terrain-fixed* push-off policy (main text Fig. 2d). Thus, in contrast to the *terrain-fixed* push-off policy, open-loop runners with the *lab-fixed* push-off policy fare worse, and display differing trends in how stability is determined by the collision parameters. However, similar to the *terrain-fixed* push-off policy, varying parameters governing the passive collision, ϵ_n and ϵ_{tc} , results in only a small effect on the mean steps to failure compared to anticipatory runners.

S9.2 Anticipatory runners

Anticipatory runners with a *lab-fixed* push-off policy increase steps taken as energy dissipation in the direction normal to the terrain surface is reduced, similar to open-loop runners with the same push-off policy. Like for the open-loop runners, this is in contrast to the trend observed for anticipatory runners with the *terrain-fixed* push-off policy, where increasing normal energy dissipation increases mean steps to failure (main text Fig. 3a). Anticipatory runners fail by losing orientational stability for a vast majority of values of the collision parameters, and orientation is maintained only when $\epsilon_{tc} = 1$ and $\epsilon_n = 1$ (Fig. S11a) in contrast to the *terrain-fixed* push-off policy where anticipatory runners maintain orientation when $\epsilon_{tc} = 1$, and regardless of the value of ϵ_n (main text Fig. 3a). At $\epsilon_{tc} = 1$, anticipatory runners with a *lab-fixed* push-off, increase mean steps taken by over 4-fold, from 7 to over 30 for a 100% reduction in normal energy dissipation from $\epsilon_n = 0$ to $\epsilon_n = 1$ (Fig. S11c).

Reducing the tangential collisional impulse at landing increases mean steps to failure for the anticipatory runner with a *lab-fixed* push-off if ϵ_n is sufficiently high, while showing the opposite trend below that ϵ_n value (Fig. S11d). This is in contrast to the trend observed in anticipatory runners with the *terrain-fixed* push-off policy where mean steps taken always increases with reduced normal energy dissipation (main text Fig. 3a).

Anticipatory runners with a *lab-fixed* push-off policy perform best when $\epsilon_{tc} = 1, \epsilon_n = 0$ and worst when $\epsilon_{tc} = 1, \epsilon_n = 0$. The *lab-fixed* push-off policy is consistently worse in terms of stability than the *terrain-fixed* push-off policy for a given pair of $\epsilon_{tc}, \epsilon_n$ values except for $\epsilon_{tc} = 1, \epsilon_n = 1$ where both push-off policies are identical, as this corresponds to $\mathbf{J}_{imp} = 0$ in both.

Running with non-zero tangential collisions is optimal in the presence of sensorimotor noise (Fig. S12a). Sensorimotor noise is modeled as additive noise to ϵ_{tc} as described in main text section 3.5. This trend is similar to that found with the *terrain-fixed* push-off policy (main text Fig. 3b).

S9.3 Scaling analysis of mean steps taken

The mean statistics for the steps to orientational failure on rough terrains are predicted by the orientation change over a single step relative to the failure bound $\phi_{tol}/\phi_{\bullet}$ (Fig. S12c,d). The loss of forward speed relative to initial forward speed ($v_{x0}/\Delta v_x$) predicts failure statistics due to losing translational stability for anticipatory runners with $\epsilon_{tc} = 1, \epsilon_n = 1$ (Fig. S12b). These trends are

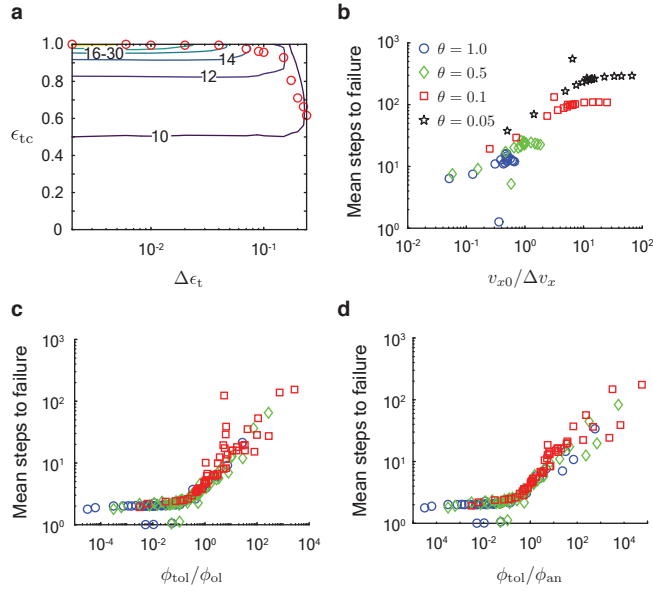


Figure S12: Effect of sensorimotor noise on stability, and scaling analysis of mean steps to failure. **a**, Contour map of mean steps taken as a function of ϵ_{tc} and $\Delta\epsilon_t$ shows that mean steps to failure reduces with increasing sensorimotor noise $\Delta\epsilon_t$. Scuffing the ground upon landing is optimal as noise intensity $\Delta\epsilon_t$ is increased. Red circles denote the optimal ϵ_{tc} value for a given $\Delta\epsilon_t$. In these simulations $\epsilon_n = 1$. **b**, For the anticipatory runner with $\epsilon_{tc} = 1, \epsilon_n = 1$, the mean steps to translational failure are predicted by the parameter $v_{x0}/\Delta v_x$. The values of the remaining parameters used in this simulation are shown in Fig. S7. Mean steps to orientation failure are captured by the parameter **c** ϕ_{tol}/ϕ_{ol} for the open-loop runner, and by **d** ϕ_{tol}/ϕ_{an} , for the anticipatory runner. The parameter values used for these simulations are shown in Fig. S7.

similar to those observed for the runner with a *terrain-fixed* push-off policy (main text Fig. 6), although there is a greater spread in the data about the trend line with the *lab-fixed* push-off.